

See discussions, stats, and author profiles for this publication at: <https://www.researchgate.net/publication/375983334>

Recent Progress of Vertical Graphene: Preparation, Structure Engineering, and Emerging Energy Applications

Article in Small · November 2023

DOI: 10.1002/sml.202307923

CITATIONS

0

5 authors, including:



Zhiheng Wu

Zhengzhou University

23 PUBLICATIONS 414 CITATIONS

SEE PROFILE



Shen Yonglong

Zhengzhou University

56 PUBLICATIONS 1,433 CITATIONS

SEE PROFILE

READS

22



Zhang Gongkai

Tianjin University

2 PUBLICATIONS 18 CITATIONS

SEE PROFILE



Guosheng Shao

Zhengzhou Materials Genome Institute

178 PUBLICATIONS 4,031 CITATIONS

SEE PROFILE

Recent Progress of Vertical Graphene: Preparation, Structure Engineering, and Emerging Energy Applications

Zhiheng Wu, Erhao Wang, Gongkai Zhang, Yonglong Shen, and Guosheng Shao*

Vertical graphene (VG) nanosheets have garnered significant attention in the field of electrochemical energy applications, such as supercapacitors, electro-catalysis, and metal-ion batteries. The distinctive structures of VG, including vertically oriented morphology, exposed, and extended edges, and separated few-layer graphene nanosheets, have endowed VG with superior electrode reaction kinetics and mass/electron transportation compared to other graphene-based nanostructures. Therefore, gaining insight into the structure-activity relationship of VG and VG-based materials is crucial for enhancing device performance and expanding their applications in the energy field. In this review, the authors first summarize the fabrication methods of VG structures, including solution-based, and vacuum-based techniques. The study then focuses on structural modulations through plasma-enhanced chemical vapor deposition (PECVD) to tailor defects and morphology, aiming to obtain desirable architectures. Additionally, a comprehensive overview of the applications of VG and VG-based hybrids in the energy field is provided, considering the arrangement and optimization of their structures. Finally, the challenges and future prospects of VG-based energy-related applications are discussed.

causing harm to the environment.^[2–4] In these devices, renewable energy sources can be stored in the form of chemical energy, which can then be rapidly converted into clean electricity. The efficiency of these electrochemical reactions is often hindered by reaction kinetics, making it crucial to identify suitable electrode materials (including anodes, cathodes, and catalysts) that can minimize reaction barriers and accelerate the overall electrochemical process.^[5,6] Therefore, the rational design and preparation of these electrode materials play a vital role in the advancement of energy storage and conversion systems.

Graphene and graphene-related materials have been widely used in diverse energy storage and conversion devices as main active materials, additives, or scaffolds in electrodes, owing to their exceptional properties such as high mechanical strength, supreme electron mobility, huge specific surface area, and facile functionalization.^[7–9] However, the design of electrode materials with tailored

1. Introduction

Over the past few centuries, the rapid development of industry and society has led to an increasing demand for energy, primarily sourced from conventional fossil fuels that are depleting at an alarming rate.^[1] This situation necessitates urgent exploration of high-performance, cost-effective, and environmentally friendly electrochemical energy storage and conversion devices. These devices include solar cells, rechargeable batteries, supercapacitors, fuel cells, and water electrolysis systems, all of which aim to enable efficient energy storage and conversion without

chemical properties and morphology is still challenging for enhancing the performance of energy devices by improving reaction kinetics and mass/electron transfer capability.^[10] A feasible approach to addressing this issue is endowing graphene with new structure characteristics, such as doping with heteroatoms and 3D architectures, which are beneficial to electrochemical systems.^[11,12] Conventional laid-down graphene-like powder and chemically reduced graphene oxide are mostly derived from high-temperature pyrolysis and chemical treatment.^[7,13,14] However, these processes often result in rather poor crystallinity, which leads to agglomeration and seriously hindered ion and charge transport in electrochemical devices. Therefore, in order to realize high electrode reaction activity, it is necessary to design graphene structures that allow efficient planar electron transport while minimizing steric hindrance.

Compared with laid-down graphene, vertical graphene (VG) is composed of folded graphene nanosheets with seamless edges, exposed surfaces, and grown perpendicularly to the substrates.^[10,15] Although VG on various substrates can have petal-like, flakes-like, maze-like, highly-branched morphology,^[16–19] in the form of VG nanosheets,^[19,20] VG arrays,^[21,22] VG nanowalls,^[23] vertically aligned reduced graphene oxide,^[24,25] each nanosheet possesses a self-supported structure with outstanding electronic and mechanical properties

Z. Wu, E. Wang, G. Zhang, Y. Shen, G. Shao
State Centre for International Cooperation on Designer Low-carbon and Environmental Materials (CDLCEM)
School of Materials Science and Engineering
Zhengzhou University
100 Kexue Avenue, Zhengzhou 450001, China
E-mail: gsshao@zzu.edu.cn

Z. Wu, Y. Shen, G. Shao
Zhengzhou Materials Genome Institute (ZMGI)
Building 2, Zhongyuanzhigu, Xingyang, Zhengzhou 450100, China

The ORCID identification number(s) for the author(s) of this article can be found under <https://doi.org/10.1002/sml.202307923>

DOI: 10.1002/sml.202307923

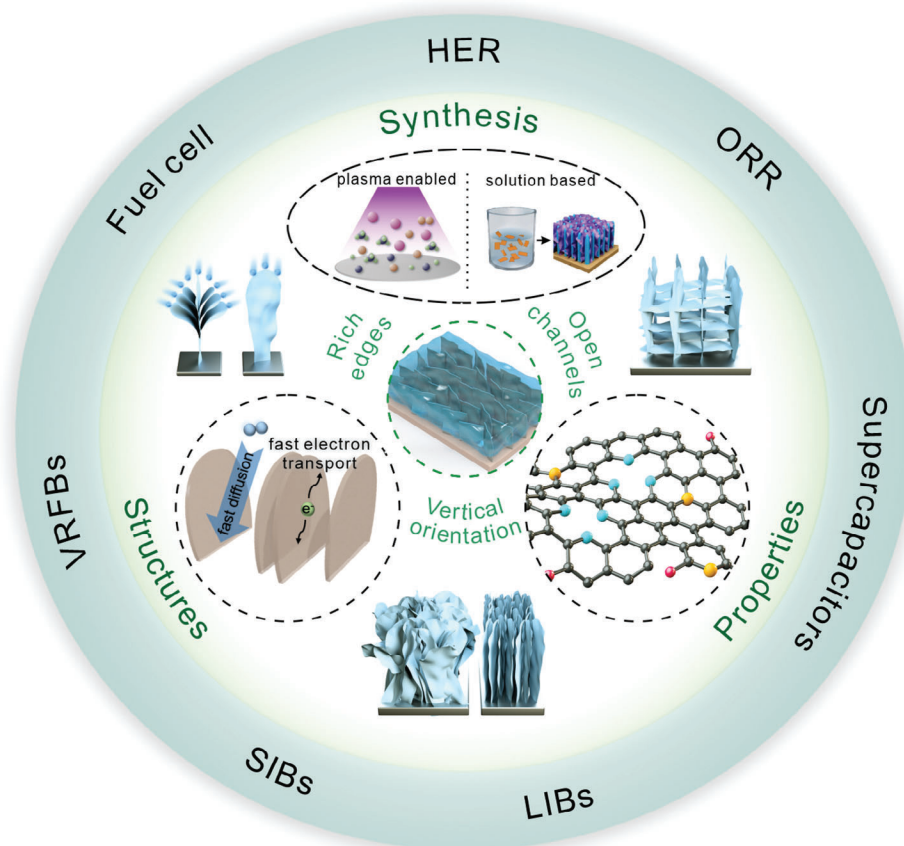


Figure 1. Schematic illustration of the synthesis, structure features, and related applications of vertical graphene.

characteristic of 2D graphene or graphene like materials. Notably, VG and its related structures have attracted tremendous interests in emitters,^[26] supercapacitors,^[24] rechargeable batteries,^[27] and electrocatalysis,^[28] owing to their distinct structure features: a) vertical standing orientation that aligns with the direction of ion and electron transfer between electrodes, b) abundant edge defects directly exposed in electrolytes, facilitating active sites for electrochemical reactions, and c) non-aggregating morphology with separated open channels, which ensure stable and efficient mass transfer pathways. Considering these advantages, it is of vital importance to focus on assembly strategies and arrangement of VG for real device applications.

Although there have been several reviews on VG and its applications,^[29,10,15,30–33] few is devoted to rational design of VG defects and morphology specially in the energy field. This review article focuses on the construction of desirable architectures in terms of controllable preparation and structural modulation for energy application, as illustrated in **Figure 1**. The main preparation strategy of VG is laid on solution-based methods and vacuum-based methods. In solution-based techniques, VG fabricated from graphene oxide or organics after pyrolysis, template-based formation, hand-rolling and cutting, and self-assembly will be briefly discussed. Vacuum-based methods mainly cover the plasma-enhanced chemical vapor deposition (PECVD) technique. This article summarizes recent advances in PECVD systems and the growth mechanism of VG in a plasma environment.

More importantly, the structural engineering of VG, with useful intrinsic defects aheteroatom-doped defects, and as well as morphology arrangement governed by various growing parameters, is discussed in detail. , This review then highlights the state-of-the-art development of novel VG based electrode materials that are fabricated for practical use in energy storage and conversion devices and discusses the decisive roles of VG, both directly as active materials themselves or scaffolds to load other active materials. Finally, the review provides an overview of the current progress and remaining challenges in the use of VG for energy applications. It also offers insights into the future development of novel VG-based electrochemical electrode materials.

2. Synthesis Methods

In solution-based methods, various forms of vertically aligned graphene-like materials, such as nanosheets,^[19,20] arrays,^[21,22] nanowalls,^[23] vertically aligned reduced graphene oxide,^[24,25] are typically fabricated from organic materials^[34,35] or reduced graphene oxide^[24,25,36–38] through processes like pyrolysis, template-based formation, hand-rolling and cutting, and self-assembly. These processes always involve high-temperature annealing to enhance graphitization and determine the final structure of VG. In contrast, the vacuum-based method involves the arrangement of carbon atoms or fragments dissociated

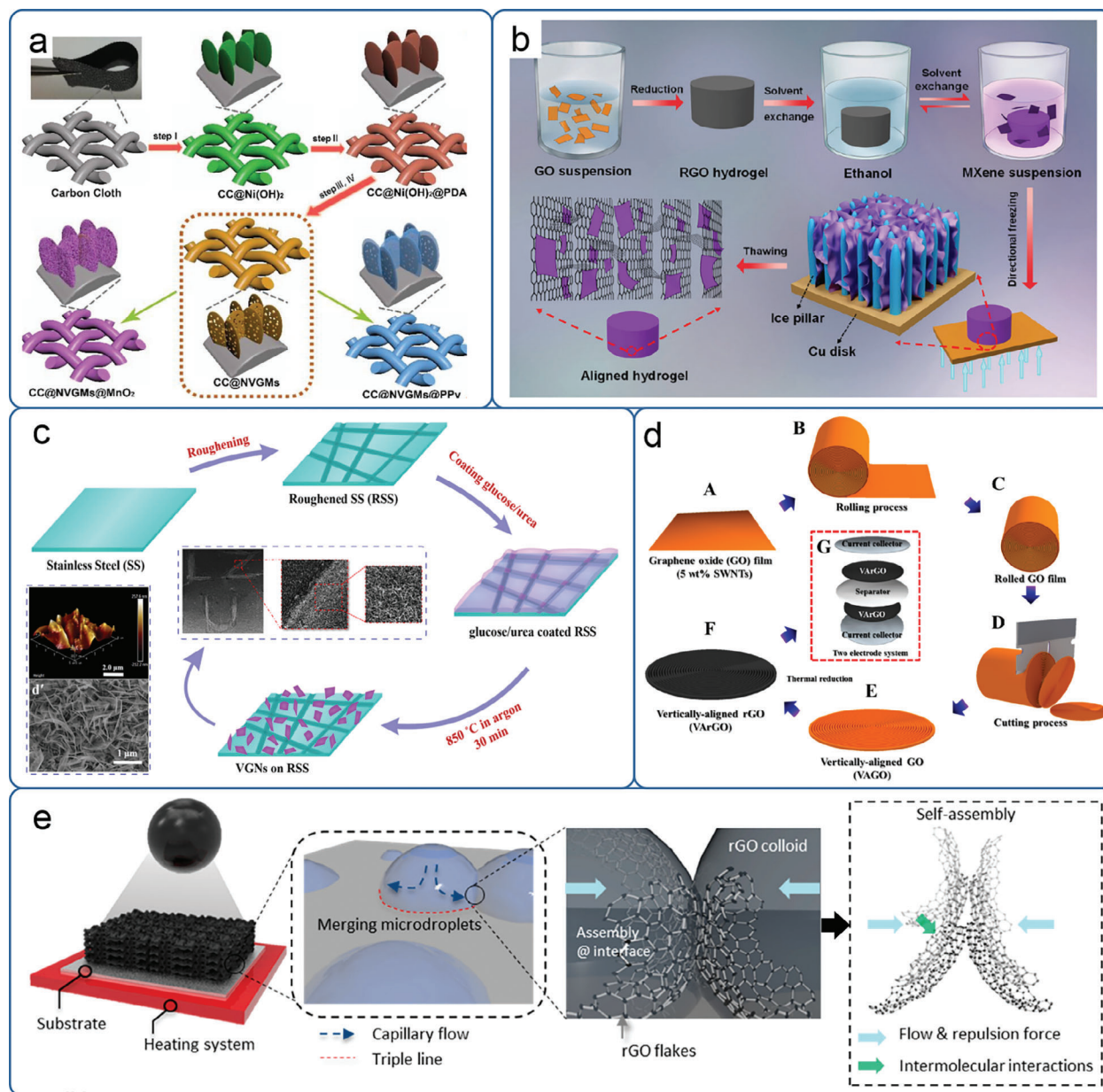


Figure 2. Solution-based methods for fabrication of VG. a,b) Template-based method. a) Reproduced with permission.^[34] Copyright 2019, Wiley-VCH. b) Reproduced with permission.^[25] Copyright 2020, Springer. c) Pyrolysis method. Reproduced with permission.^[35] Copyright 2018, Elsevier. d) Hand-rolling and cutting method. Reproduced with permission.^[24] Copyright 2014, American Chemical Society. e) Self-assembly method. Reproduced with permission.^[38] Copyright 2021, American Chemical Society.

from gas/solid precursors into a principally crystalline graphene structure from the gas phase.

2.1. Solution-Based Methods

2.1.1. Template-Based Method

Various solution-based strategies are used to grow vertical graphene (VG), including the template-based method utilizing etchable scaffold with vertical orientation or directional freez-

ing ice. For instance, Wang and colleagues developed a self-sacrificing template method for fabricating N-doped porous vertical graphene-like nanomesh arrays (NVGMs) on a flexible carbon cloth substrate, as shown in Figure 2a.^[34] In this process, Ni(OH)₂ nanosheets templates were grown on carbon cloth by hydrothermal method with vertical orientation, followed by polydopamine (PDA) coating and carbonization heat treatment. Afterward, the Ni particles were removed by soaking the sample in an acid solution to obtain the vertical graphene nanomesh arrays. However, the etchable scaffold still inevitably brings impurities, which could cause device failure or safety issues in batteries. To

overcome this, directional-freezing technology has proven to be an efficient method to grow VG, since the ice is always used as the template and sublimate easily in vacuum environment.^[25,39] As shown in Figure 2b, Yu and coworkers used a liquid nitrogen-assisted directional-freezing technique to grow vertically oriented ice pillar from the bottom of RGO/MXene hydrogel. During the freezing process, the RGO/MXene hydrogel was expelled and aligned along the vertical oriented pillars. Upon thawing of the hybrid hydrogel, the vertical graphene-like composite was obtained.^[25]

2.1.2. Pyrolysis Method

The pyrolysis method is a cost-effective and straightforward approach used for synthesizing VG, compared to other methods. In this method, pyrolysis is always conducted to accelerate the decomposition of organic polymer materials and promote the growth of VG.^[35,40] Figure 2c demonstrates the typical pyrolysis strategy on roughed stainless steel.^[35] In this strategy, glucose and urea were introduced as precursors and then elevated to 850 °C in low pressure on a roughed stainless steel, which provides abundant nucleation sites for VG growth. The growth of VG can be attributed to different nucleation and growth rates on the pre-treated substrate, which is similar to that of thermal chemical vapor deposition (CVD).^[41] More details about the growth mechanism will be described in the following section.

2.1.3. Hand-Rolling and Cutting Method

Vertically oriented morphology can also be fabricated through the direct cutting from rolled graphene oxide (GO) film, as shown in Figure 2d. Lee and coworkers tightly rolled wet GO films and cut specimen into thin pieces (within 10 μm) using a rotary cryomicrotome. Finally, cut sections were annealed at 1000 °C and reduced to obtain vertically aligned rGO films.^[24] Bai and coworkers further introduced vertically aligned graphene film/liquid polydimethylsiloxane (PDMS) and thermally reduced vertically aligned reduced graphene oxide/epoxy composite in the rolling and cutting routine.^[42,43] The thermal conductivity of resulting material have demonstrated significant enhancement of per wt.% of as high as 3329% compared to pure PDMS and 887% compared to pure epoxy. These improvements were attributed to the vertical alignment of graphene-like films and high in-plane thermal conductivity.

2.1.4. Self-Assembly Method

As shown in Figure 2e, Ahn and coworkers proposed an advanced boiling method, which involves spraying a reduced graphene oxide (rGO) colloid in microdroplets onto a heated target substrate. The rapid vaporization of the liquid films on the substrate forces the rGO sheets arranged at the liquid-vapor interface, finally leading to the self-assembly of vertical structure.^[38] In another approach, Hurt and coworkers used sulfonated polyaromatic dyes with a hydrophilic periphery and hydrophobic core as the liquid crystal phase to retain supramolecular alignment even after carbonization. These water-soluble dyes, acting as supramolecular

rods, can order into parallel orientation and produce a set of vertically aligned disks at high concentration. After carbonization, the disks are converted into vertically oriented graphene structures, resulting in a final product with desirable properties.^[44]

2.2. Vacuum-Based Methods

Compared with thermal CVD (T-CVD),^[27,41] PECVD is the principal technique used for VG fabrication currently,^[15,17,37,45–47] because of its intriguing merits of low substrate temperature,^[15] catalyst-free substrates,^[18] high growth rate,^[48] and well-controlled conditions for nanostructure ordering.^[45] However, the growth of VG in PECVD is quite a complex process influenced by several factors including plasma source,^[19,49] gas precursor and ratio,^[50] and substrate temperature,^[51] and consequently the morphology and defects of the VG are significantly affected, which can complicate the growth mechanism and make it challenging to design structures for various applications.

2.2.1. Recent Advances in PECVD System for VG Growth

Petal-like VG structure was first observed on the graphite cathode during DC arc-discharge while growing carbon nanotubes.^[53] Soon afterward, it was found that VG nanowalls could also be grown on catalyst coated substrates using microwave plasma.^[54] Since then, strenuous efforts have been made to develop advanced plasma systems capable of producing highly aligned, super tall VG with high growth rate and low substrate temperature for mass production.

Microwave plasma is a powerful gas discharge plasma that operates at frequencies in the GHz range (typically at 2.45 GHz). It is characterized by its confinement in a relatively small area. Microwave plasma has been widely used for the fabrication of various carbon materials, including 1D carbon nanotube,^[55,56] 2D graphene,^[57,58] and VG^[46,59] materials, owing to the high plasma density ($\approx 10^{12}$ cm⁻³) and high ionization rate. Recently, Bo and coworkers proposed a multi-linear antenna microwave plasma based on surface wave plasma.^[60] This novel design enables the production of vertical graphene from greenhouse gases (such as CO₂ and CH₄) for energy storage applications. The process can be carried out in an industry-relevant roll-to-roll process, as depicted in Figure 3a.^[52]

The most commonly used plasma systems for VG are those operated in the radio frequency (RF) region (typically at 13.56 MHz). These RF plasma systems can be categorized into two main types: inductively coupled plasma (ICP) and capacitively coupled plasma (CCP). ICP utilizes a helical or spiral-like conductor arranged in either a planar coil or cylindrical tube geometry to couple the plasma. On the other hand, CCP consists of a pair of parallel plane electrodes.^[15,61]

Compared with CCP, ICP is more commonly used for VG growth with a relatively larger plasma volume and higher electron density.^[62] In an ICP plasma system, electric field is also introduced during the VG growth for morphology regulation, since the intrinsic electric field in plasma sheath could drive the VG curling up.^[21,45,63–65] Zhang and coworkers demonstrated an electric-field-assisted PECVD, as shown in Figure 3b.^[21] They

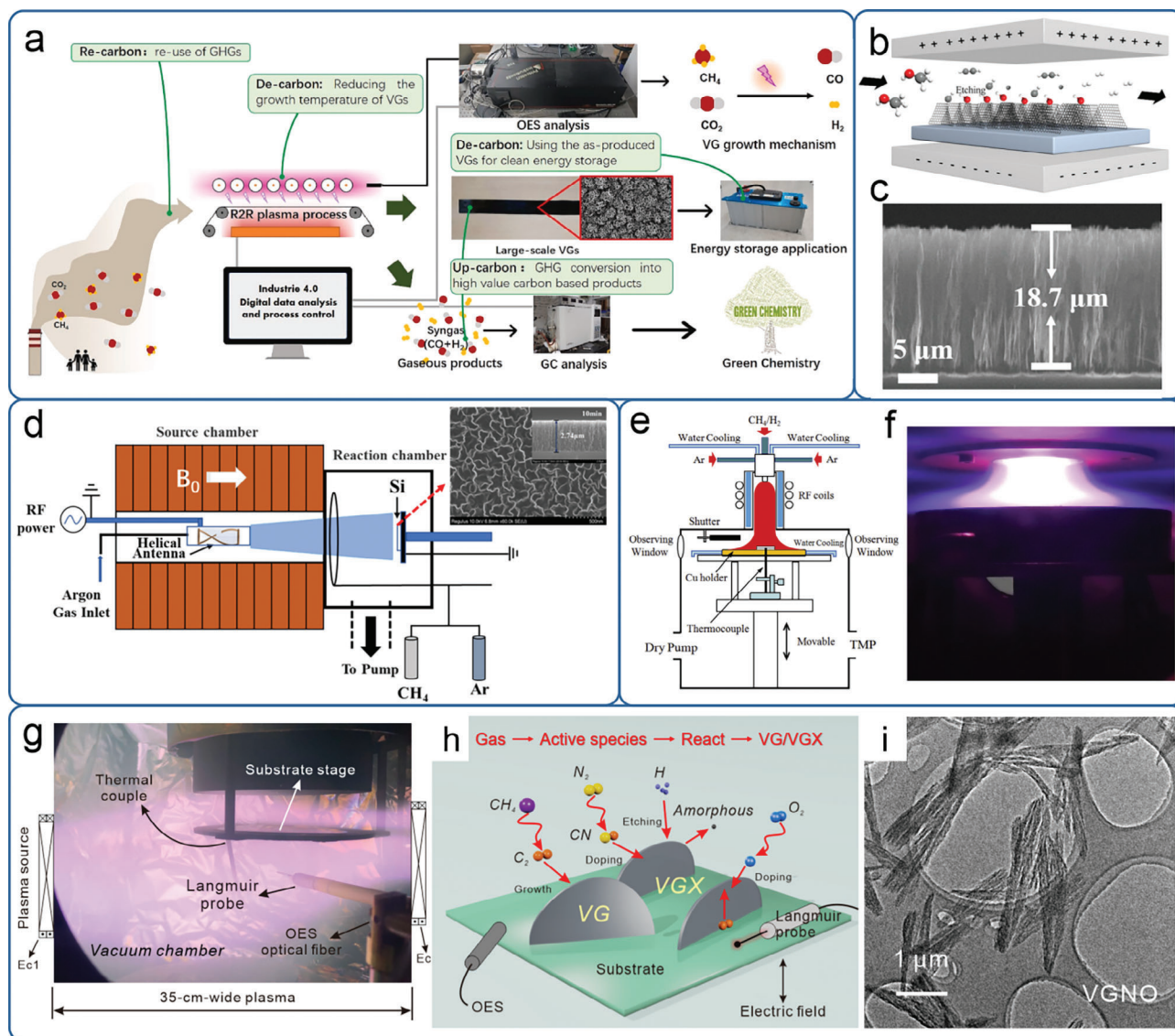


Figure 3. Vacuum-based methods for fabrication of VG. a) Illustration of the pilot-scale roll-to-roll low-temperature plasma process simultaneously producing VG and related applications. Reproduced with permission.^[52] Copyright 2022, Elsevier. b) Schematic illustration of an electric-field-assisted PECVD system, c) cross-sectional SEM image of fabricated VG arrays. b,c) Reproduced with permission.^[21] Copyright 2020, Wiley-VCH. d) Schematic of the helicon wave plasma chemical vapor deposition (HWP-CVD) apparatus, the insert is SEM image of fabricated VG. Reproduced with permission.^[20] Copyright 2020, Elsevier. e) Schematic of the mesoplasma CVD, f) typical optical emissions in mesoplasma. e,f) Reproduced with permission.^[19] Copyright 2019, Elsevier. g) Photo of the plasma optical emissions in high-flux PECVD (HPECVD) system, h) schematic illustration of the growth of VG and heteroatom-doped VG (VGX), i) a typical TEM image of nitrogen and oxygen co-doped VG. g–i) Reproduced with permission.^[49] Copyright 2022, Wiley-VCH.

found that a moderate electric field applied onto substrates could maintain a continuous growth and highly ordered vertical alignment structure with length up to 18.7 μm in 6 h fabrication (Figure 3c). When the electric field is applied perpendicular to the substrate, net charges will accumulate at the edge of VG structure. These charges can attract carbon cations along the electric field and result in an extended growth of VG instead of edge saturation.

Introducing a helical antenna and a static magnetic field in ICP will result in high plasma density ($\geq 10^{13} \text{ m}^{-3}$) and high ionization rate, consequently, VG can grow at a relatively low substrate

temperature even without the introduction of extra amorphous carbon etchant (H_2 , O_2 , etc.).^[20,66] Figure 3d shows a typical helicon wave plasma CVD apparatus.^[20] The VG can grow on Si substrates forming a uniform, ordered, and compact cavity structure without catalyst and joule heating at a high average growth rate of $0.26 \mu\text{m min}^{-1}$, which was attributed to rich active radicals, inherent electric field and residual stress on Si substrate in high density plasma.

Another method for the rapid and controllable growth of Vertical Graphene (VG) is the ICP-jet plasma system, also known as mesoplasma. This system utilizes a spiral-coil circled quartz

Table 1. Unique advantages and existing issues for different VG synthesis methods.

Method		Unique advantages	Existing issues
Solution-based	Template-based	Morphology controllable;	Susceptibility to contamination;
		Free-standing growth.	Template removal complexity.
	Pyrolysis	Cost-effective and straightforward;	Substrate constraint;
	Hand-rolling and Cutting	Uniform distribution.	Harsh growth condition.
		Excellent vertical alignment;	Complicated synthesis process;
Vacuum-based		Height controllable.	Poor layer number control.
	Self-assembly	Population controllable;	Low mass yield;
		Efficient pore structure regulation.	Inferior vertical alignment.
	T-CVD	High quality;	Limited morphology control;
		Precise dopant control.	Substrate constraint.
	MW-PECVD	Catalysts-free;	High equipment cost;
	RF-PECVD	Free of substrate heating.	Poor uniformity.
		Large-scale fabrication;	Low growth rate;
		Simple growth equipment.	Complex control requirement.

tube and requires a relatively high power input.^[19,67] Figure 3e,f shows a typical mesoplasma CVD system and corresponding images of Ar-H₂-CH₄ mesoplasma optical emissions. In this system, a compact cauliflower-like VG structure was uniformly distributed on silicon substrates with an ultra-high growth rate of 18.01 μm min⁻¹, which was attributed to high flux plasma operated at a high working pressure (800 Pa) and high plasma power input (tens of kW).^[19] The sheet density can reached $\approx 2.0 \times 10^{10}$ cm⁻² and the mass loading in unit area per minute increased to 0.112 mg cm⁻² at 18 kW. These values demonstrate high growth efficiency and significant variation in the film structure.

The recently reported high-flux PECVD (HPECVD) system, assisted by in situ plasma diagnostics, enables the fabrication of vertically aligned graphene (VG) on stainless steel substrate without the need for a heater.^[49] As shown in Figure 3g, electrons and ions are guided and confined to “spiral” paths around the streamlined magnetic field produced by static magnetic coil placed at the entry and the other side of the chamber. Meanwhile, this HPECVD was equipped with plasma diagnostics consisting of a Langmuir probe and optical emission spectrometer. Such a HPECVD system shows several advantages: a) providing stable and high density plasma (10¹² cm⁻³) for uniform growth of VG without substrate heating,^[68] b) versatile growing parameters tuning the morphology and doping states, c) the growing and doping processes can be in situ monitored in terms of plasma radicals and parameters for optimized practical performance (Figure 3h). Meanwhile, the real-time plasma monitoring ensured the optimization of plasma constituents, densities, and radicals. This ensures the fabrication of nitrogen and oxygen co-doped VG with perfect vertical orientation, controllable doping states, and enhanced reaction kinetics in electrocatalysis (Figure 3i). The unique advantages and current issues of each synthesis methods are presented in Table 1.

2.2.2. Growth Mechanism of VG in PECVD

In the thermal CVD process, the hydrocarbon precursors are decomposed into carbon species on the surface of transition metals such as copper or nickel, typically at high temperature exceeding 1000 °C. The carbon species subsequently nucleate, grow, and coalesce to form a continuous film, following a near thermodynamic equilibrium pathway.^[69] On contrary, PECVD enabled VG growth is quite different from that of thermal CVD. In PECVD, hydrocarbon precursors undergo ionization and dissociation due to energetic electrons generated in the plasma at relatively low temperature.^[70] The growth of the film is far from reaching thermodynamic equilibrium, with the entire process being largely influenced by kinetics.^[71] In this process, a widely accepted growth mechanism of VG in terms of nucleation-growth-termination was proposed as follows:

- Nucleation:** In the early stage, a buffer layer was formed on the substrate as the nucleation for incoming carbon radicals (Figure 4a).^[72] This buffer layer consists of amorphous carbon or carbide composite, mainly due to insufficient time and temperature for complete graphitization (Figure 4b).^[76] It has been reported that the carbide composites formed on the substrate of Si, Mo, and Ni, as carbon atoms concurrently dissolve into the interstices of the metal or exhibit a tendency to form carbides. The buffer layer plays a crucial role in enhancing the adhesion between the VG and the substrate.^[51,77,78] However, it is worth noting that the mismatch between amorphous carbon/carbide composite and graphitic layer could incubate nucleation sites and promote the population of VG growth (Figure 4c).^[73]
- Growth:** After the nucleation process, the VG plane continues to grow perpendicular to the substrate, mainly following

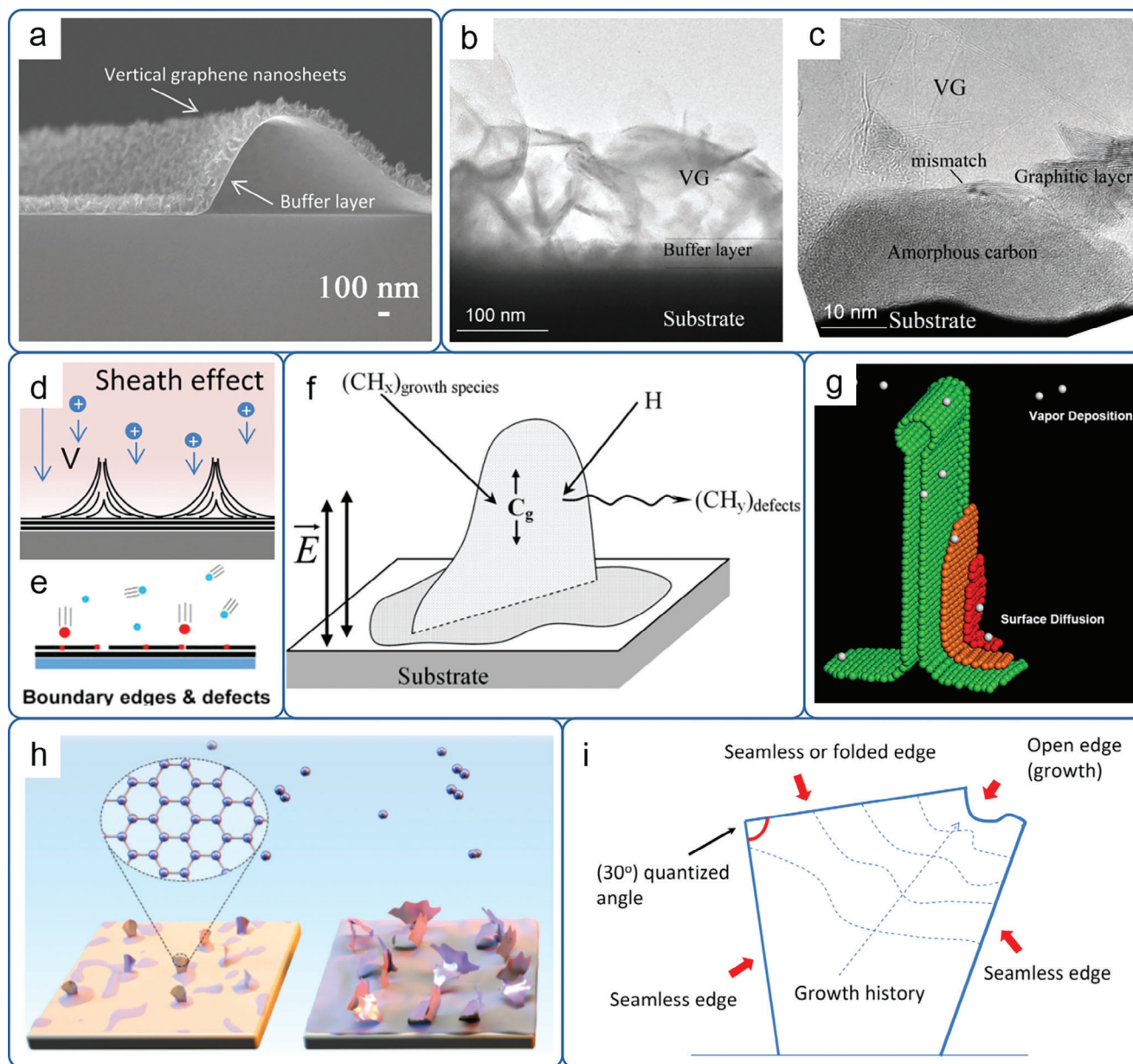


Figure 4. VG growth mechanism. a) The SEM image of vertical graphene nanosheets and buffer layer on substrate. Reproduced under terms of the CC-BY license.^[72] Copyright 2015, Springer. b,c) TEM images show the amorphous carbon on substrate as the buffer layer and nucleation sites for graphite layer formation. b,c) Reproduced with permission.^[73] Copyright 2014, American Chemical Society. d) The basal graphite plane grows perpendicular to substrate under the sheath effect in plasma system. Reproduced under terms of the CC-BY license.^[72] Copyright 2015, Springer. e) Strain effect in the edge and defects help graphene grow vertically. Reproduced with permission.^[74] Copyright 2019, American Chemical Society. f) VG growth controlled by electric field and carbon surface diffusion. Reproduced with permission.^[75] Copyright 2007, Elsevier. g) A continuum model based on the surface diffusion. Reproduced with permission.^[73] Copyright 2014, American Chemical Society. h) A schematic of nucleation and growth process in HPECVD system. Reproduced with permission.^[68] Copyright 2020, Wiley-VCH. i) Schematic showing VG growth terminated with seamless or folded edge. Reproduced with permission.^[76] Copyright 2014, Elsevier.

two mechanisms in terms of electric field effect and strain effect. As shown in Figure 4d, the local electric field generated by plasma sheath and substrate biasing could facilitate higher charge transfer capacity in line with the electric field.^[45,65,72] The radically higher charge transfer capacity along the basal plane allows for a greater storage of charges and carbon cations at the edge, thereby facilitating the verti-

cal growth of VG.^[21] Moreover, the strain accumulated within the graphene domain, induced by the temperature gradient and the mismatch between substrate and buffer layer, generates an upward force perpendicular to the substrate. Over time, this upward force steadily accumulates, resulting in the alignment and ordering of VG,^[45] which can also account for the growth of VG in thermal CVD^[41] and in high-temperature

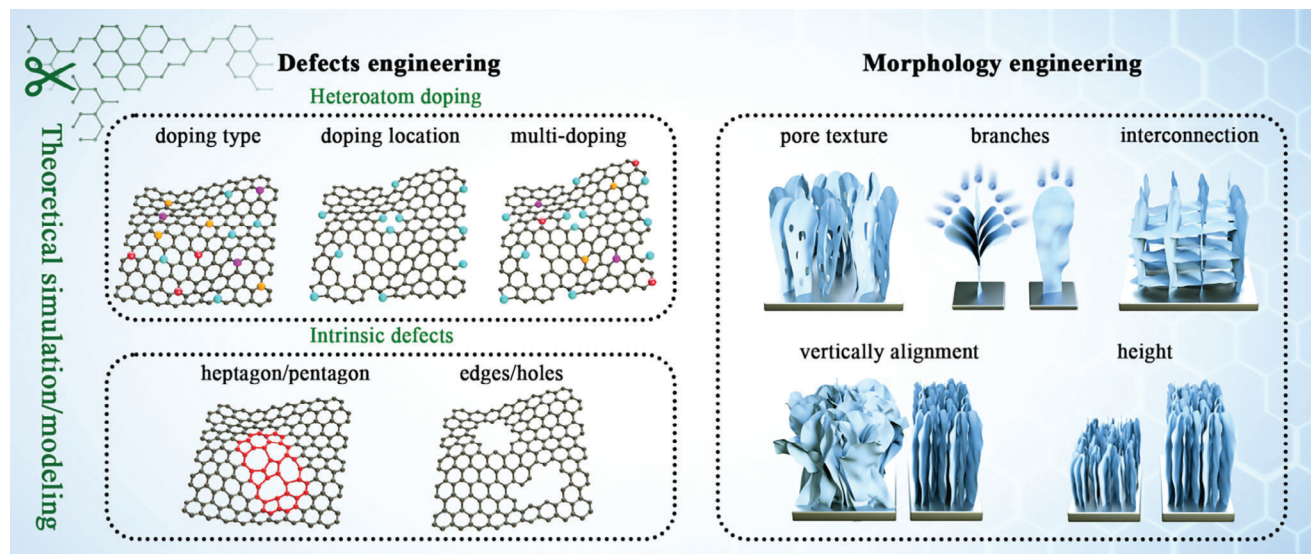


Figure 5. Structure design principles for VG.

pyrolysis^[35] even in the absence of an electric field (Figure 4e). It was also reported the vertical growth of VG on dielectric substrates was attributed to a combination of electric field effect and strain effect.^[79]

The surface diffusion of carbon atoms is a key factor in the growth of VG, which results in the anisotropic growth of VG along or perpendicular to basal plane. It can be enhanced by two factors: electric-field induced polarization effects and high substrate temperature (above 1000 K), as shown in Figure 4f. The surface diffusion energy of carbon atoms was reported ten times higher than the surface adsorption energy, resulting in faster in-plane growth instead of thickening.^[75] In this condition, the surface diffusion and growth of carbon (adatom) on substrates can be considered as a step-flow mode process.^[73] The steps formed in this model act as the active edges that facilitate vertical growth and lip-lip connection, terminating further growth (Figure 4g). Nevertheless, the VG growth at relatively low substrate temperature (<600 K) exhibits a different phenomenon, as illustrated in Figure 4h. In high-flux PECVD, the plasma density is similar to that in microwave plasma enhanced CVD.^[49] In this high density plasma condition, the nucleation and growth process are primarily influenced by the plasma, allowing VG to vertically grow through promoted nucleation and limited surface diffusion simultaneously, which is similar with the report that the growth is determined by the direct attachment of carbon radicals to VG edges.^[77]

- iii) Termination: The reported termination of VG growth was influenced by different type of edges, namely open edges, and seamless/folded edges, as shown in Figure 4i. The presence of amorphous carbon and defects in graphene structure would disturb the formation of sp^2 lattices and contribute to the occurrence of seamless as well as folded edges. This bending curvature restricts the diffusion of carbon atom, leading to the termination of growth and determining the final height of VG.^[73]

Although the three-step mechanism has been supported by numerous experimental observations in PECVD process, there is still a lack of comprehensive understanding that can precisely guide VG growth precisely for rational structure design and further applications.

3. Structure Engineering of VG

VG possesses various unique structure properties, including a large surface to volume ratio, nonaggregating morphology, exposed surface, easy to be functionalized, and abundance of ultra-thin edges.^[15] These properties make VG suitable as a scaffold for loading active materials or directly participating in redox reactions. Nevertheless, these properties are strongly associated with vertical architectures,^[17] pore texture,^[80] and defect states,^[28,81,82] which can be elaborated in terms of defects and morphology aspects, as depicted in **Figure 5**. In combination with theoretical simulation and modeling using density functional theory (DFT), it is more efficient and rational to design VG materials for practical use without reliance of experiment data.^[83]

3.1. Defect Engineering

Few-layer graphene nanosheets are building blocks to vertical oriented graphene nanostructure. However, the inherent sp^2 hybridization of carbon atoms have shown inert to electrochemical reaction, leading to insufficient charge transfer effect between the carbon atoms and loaded active materials.^[84] Therefore, defects engineering in terms of both intrinsic defects and heteroatom-doped defects, is highly desirable to modulate the intramolecular charge transfer effects for functional device applications.

3.1.1. Intrinsic Defects

Intrinsic defects in graphene materials are inevitable according to the second law of thermodynamics. These defects can arise

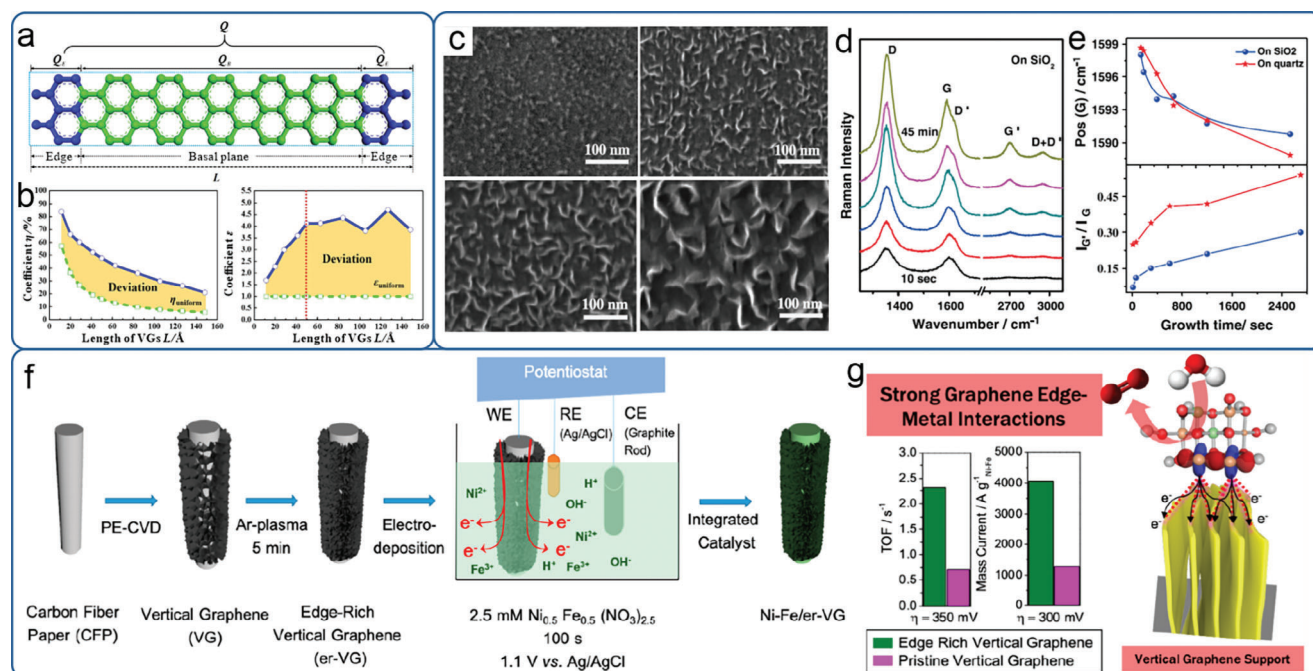


Figure 6. Intrinsic defects in VG structure. a) Schematic of zigzag VG with edge and basal plane. b) As-calculated two coefficients (η and ϵ) representing the charge storage ability. a,b) Reproduced with permission.^[82] Copyright 2016, Elsevier. c) SEM images of VG grown at different duration of 10 s, 10 min, 20 min, and 45 min. d) Raman spectra of VG grown at different duration of 10 s, 1 min, 5 min, 10 min, 20 min, and 45 min. e) Variation of G band and I_G/I_C with respect to growth time. c–e) Reproduced with permission.^[93] Copyright 2014, Wiley-VCH. f) Schematic showing the fabrication of Ni-Fe/er-VG. g) The edge rich vertical graphene shows strong interaction with the aligned Fe d_{z^2} orbital that results in excellent oxygen evolution reaction (OER) performance. f,g) Reproduced with permission.^[91] Copyright 2020, American Chemical Society.

from processes such as limited-time crystal growth, irradiation with energetic particles, and chemical/physical treatment, leading to the formation of topological defects (such as pentagons and heptagons rings) and edge defects.^[85] It has been demonstrated that VG possesses abundant tapered and ultrathin edges, which can be controlled and offer advantages in a wide range of applications.^[86,87] However, their recognition and rational modulation is still a challenge.

A proper modulation of edge density and edge-to-basal ratio is an effective strategy to enhance the predominant roles of edges. It has been reported that VG with denser edges shows superior charge storage performance.^[82] Both mass specific capacitance and area specific capacitance were calculated almost two times higher than that of the control electrode. Abundant exposed edges can not only act as active sites and store more charges, specifically, the electrons near the edges also present much faster transfer rates compared to the basal plane. The underlying mechanisms describing the charge distribution with different edge-to-basal ratios was also conducted with DFT calculations, as shown in Figure 6a,b. Both of two coefficients (η and ϵ) showed obvious deviation from the control sample, verifying the charge redistribution and accumulation in the edge regions. In this model, edges disrupt the infinite π -electron system, resulting in quasi-localized p_z orbital states of graphene edge, which enhance the kinetics of ions in electrolyte within the interior of the graphene structure.^[88] VG with various edge-to-basal ratios can be realized by simply adjusting the growth time in PECVD system. As shown in Figure 6c, the evolution of morphology showed significant variations in height as well as the density of VG nanosheets

with different growth durations. Raman spectroscopy was utilized to characterize defects and disorder structure of VG, as shown in Figure 6d,e. The increase of growth time significantly affects band position and intensity ratio in Raman spectra. The blue shift of G band position and increase of I_G/I_C both indicate the improvement of crystallinity, which may be ascribed to the decrease of edge-to-basal ratio and enhance the percentage of basal plane with respect to edges.

To construct edge-rich graphene structure, a large number of design and synthesis strategies have been developed using oxidative unzipping,^[89] ball-milling,^[90] and plasma treatment.^[91,92] It is noteworthy that the plasma-based post-treatment and one-step fabrication is a scalable and effective method to create defects in pristine VG materials. Owing to the high plasma density and ion bombardment under electric field in RF plasma, abundant smaller and thinner graphene nanoflakes emerged at the VG edges, thereby increasing the edge density and packing density (Figure 6f). It has been demonstrated that these graphene edges can interact with other active materials (electrodeposited Ni-Fe hydroxide), altering the coordination environment of unsaturated d_{z^2} orbital of Fe and promoting the formation of redox-activated Ni sites, thus enhancing electrochemical performance (Figure 6g).^[91]

3.1.2. Heteroatom-Doped Defects

Introducing heteroatoms into carbon materials is a feasible method to modulate the charge and spin of neighbor carbon

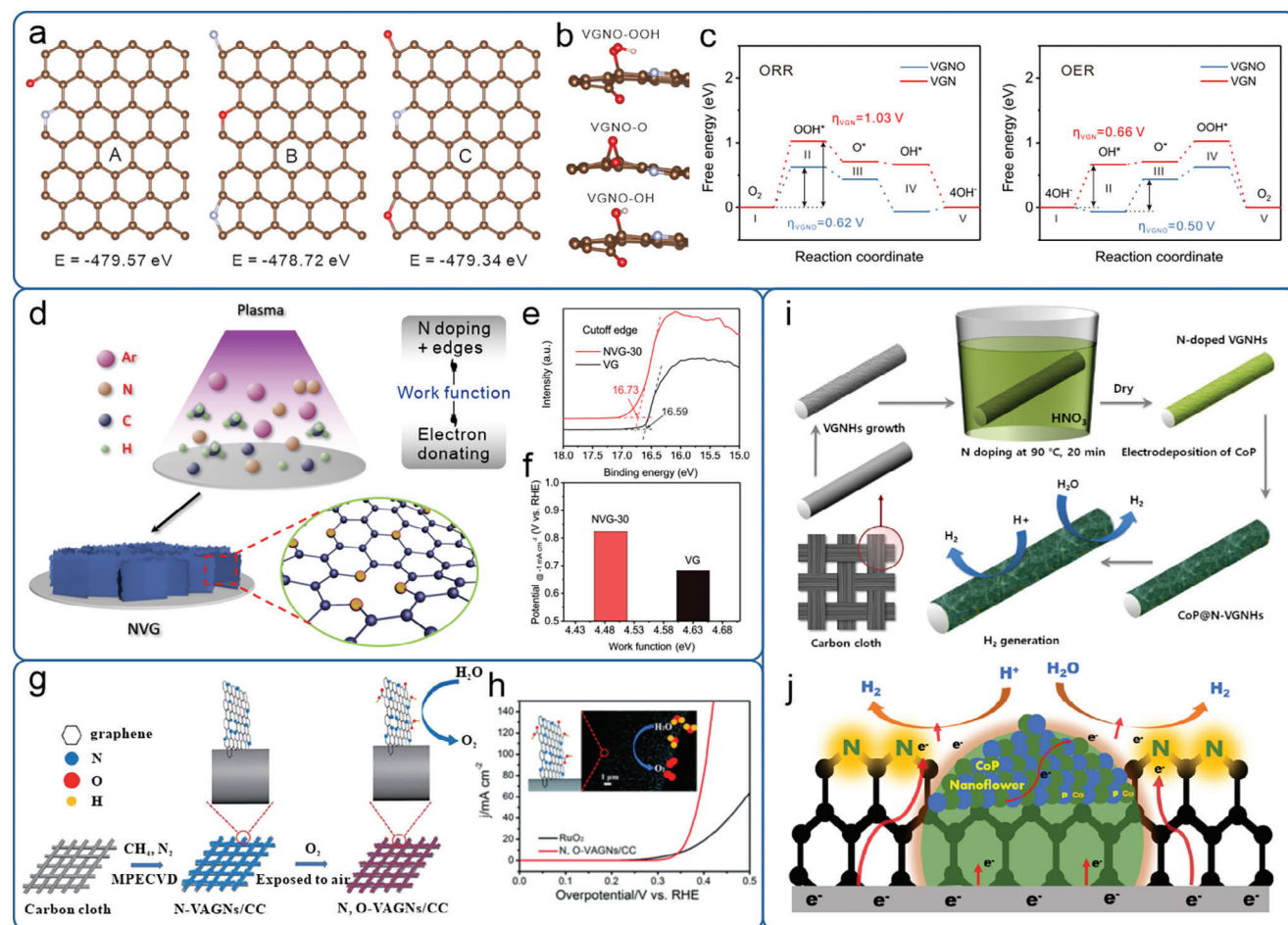


Figure 7. Heteroatom doping in VG. a) Possible nitrogen and oxygen doped VG (VGNO) with total energy obtained by density functional theory (DFT) calculation. b) Optimized structures after the adsorption of oxygen intermediates on VGNO surface. c) Energy profiles for ORR and OER pathway of VGNO. a–c) Reproduced with permission.^[49] Copyright 2022, Wiley-VCH. d) Schematic illustrating single-step fabrication of nitrogen doped VG growth in HPECVD. e, f) UPS spectra in the secondary cutoff region of VG and nitrogen doped VG revealing the relationship among nitrogen doping, work function and ORR activity. d–f) Reproduced with permission.^[80] Copyright 2020, Royal Society of Chemistry. g) Schematic showing the fabrication of N, O doped vertically aligned graphene nanosheets on carbon cloth (VAGNs/CC). h) The enhanced OER activity of N, O-VAGNs/CC with respect to commercial RuO₂ catalyst. g, h) Reproduced with permission.^[96] Copyright 2018, Royal Society of Chemistry. i) Schematic showing the fabrication of CoP hybrid nitrogen doped vertical graphene nanohills (CoP@N-VGNHs). j) Schematic illustrating the pyridinic N and CoP both contributing to the proton reduction in HER. i, j) Reproduced with permission.^[81] Copyright 2021, American Chemical Society.

atom by substituting certain carbon atoms with nitrogen,^[94] fluorine,^[95] oxygen,^[96] phosphorus,^[97] boron,^[98] sulfur,^[99] and other elements through single-, dual-, and tri-doping. The difference of electronegativity, electron affinities, atomic size, and binding state between heteroatoms and carbon atoms significantly refine charge and spin density distribution of individual atoms to impart new properties to carbon materials. Among these dopants, nitrogen is the most widely utilized in VG, owing to the facile replacement of the carbon atom for the similar atomic size and unique electronic properties derived from conjugation between long-pair electrons of nitrogen and π -electrons of graphene.^[100] Additionally, nitrogen can also coexist with other dopant such as oxygen and boron in the form of multi-atom-doped type. The synthesis strategies and applications of heteroatom doping of VG are summarized in Table 2.

Theoretical simulation and modeling in the framework of the density functional theory (DFT) toward heteroatoms doped struc-

ture enables a solid basis to design a suitable VG based electrode material for both cathode and anode in electrochemical system.^[28,47,49] Possible configurations with energetic stability and dynamical stability can be obtained, without reliance of experiment data.^[83] Based on this approach, low-energy configurations with nitrogen and oxygen dopants have been theoretically proposed, which were in agreement with experimental results (Figure 7a). Specifically, the pyridinic type of heteroatom-doped VG bonded with different oxygen intermediates showed the lowest energy barrier for oxygen reduction reaction (ORR) and oxygen evolution reaction (OER) processes in alkaline electrolyte compared to the counterpart (Figure 7b,c). Moreover, a deeper understanding of the relationship between heteroatom-doped structure and electrochemical performance may be reached, when combined with experiments and DFT calculations.

The coexistence of heteroatoms doping and intrinsic defects is commonly observed during the growth and processing of VG

Table 2. Doping strategies and applications of VG.

Material	Doping type (source)	Doping content [at. %]	Synthesis methods	Application	Ref.
Nitrogen-doped vertical graphene	N (N ₂)	6.7	Plasma	ORR catalyst	[80]
3D nitrogen-doped vertical graphene nanosheets	N (melamine)	24.33	CVD	Zn-ion battery	[101]
(N, O)-doped vertical few-layer graphene film	N (N ₂), O (O ₂)	5.1 (N), 16.7 (O)	Plasma	ORR, OER catalyst	[49]
Nitrogen-doped, oxygen-functionalized vertically aligned graphene nanosheets	N (N ₂), O (O ₂)	2.05 (N), 8.86 (O)	Plasma (N), Exposed to air (O)	OER catalyst	[96]
Nitrogen doped carbon nanowalls (CNWs)	N (N ₂)	20	Plasma	ORR catalyst	[102]
Vertical nitrogen-doped few-layer graphene	N (N ₂)	3.98	Plasma	Field emission	[46]
CoP loaded nitrogen doped vertically oriented graphene nanohills	N (HNO ₃)	1.3 (pyridinic)	Nitric acid treatment	HER	[81]
Nitrogen doped vertical graphene nanosheets	N (urea)	1.86	Pyrolysis	Field emission	[35]
B and N co-doped vertical graphene	B (B(OCH ₃) ₃), N (N ₂)	4.47 (B), 3.18 (N)	Plasma	Electroencephalogram recording	[103]
Nitrogen doped vertical graphene	N (NH ₃)	3.7	CVD	HER	[47]

materials.^[84] In the HPECVD system, the nitrogen doped VG (NVG) is fabricated using a one-step strategy (Figure 7d).^[80] In this method, fabrication parameters were rationally designed to control various properties of the VG, including height, distance between nanosheets, pore texture, interlayer spacing of graphene, as well as the degree of disorder and crystallization. Besides, the synergetic effect of edge defects and nitrogen-doping contributes to the regulation of electron donating capability by tuning the work function of NVG, as illustrated in Figure 7e. Consequently, the optimized NVG demonstrate accelerated ORR kinetics and superior activity (Figure 7f).

Beyond substitutional doping, the surface functionalization is also an effective method especially for edge-rich VG structure.^[96] The as fabricated VG in vacuum environment possesses unsaturated dangling bonds on the open edges, which can react with functional groups. As shown in Figure 7g, the nitrogen doped vertically aligned graphene nanosheets (N-VANGs) were exposed to air once after synthesis, the oxygen in the air reacted and moderately functionalized with the open surface of VANGs, leading to N, O co-doped structure. It was demonstrated that the N plasma promoted the doping content of O, as well as the defects and discontinuity in graphene structure. As a result, the introduced N and O can render the adjacent carbon atoms positively charged, resulting in enhanced OER performance (Figure 7h).

Heteroatoms doped VG can not only act as active materials in redox reactions, but also an excellent scaffold for other functional materials such as alloys,^[91] transition metal composite,^[81] metal oxides,^[104,105] and metal nanoparticles^[106] with high loading capacity. CoP nanosheets were anchored on nitrogen doped vertical graphene nanohills (N-VGNHs) structure via electrodeposition method and the morphology and doping state of N-VGNHs have been well preserved for the robust structure of VG (Figure 7i). In this hybrid structure, the N dopants significantly enhanced the charge transfer effect between graphene and CoP nanosheets, contributing to enriched active sites in HER compared with carbon cloth (CC) or undoped VGNHs. Meanwhile, the N dopants also increased the electronic conductivity of the CoP@N-VGNHs and reduced the charge transfer resistance from 4.4 to 0.9 Ω in acid and 4.4 to 2 Ω in alkaline solutions (Figure 7j).

3.2. Morphology Engineering

By virtue of the vertically standing morphology, VG has been distinguished from other graphene materials. The growth of VG in PECVD shows good controllability over morphology by adjusting various growth parameters such as plasma type, gas precursors, substrate type, substrate temperature, as shown in Table 3. Although VG can be grown on various substrates including metals,^[21,107,108] oxides,^[109,110] carbon fiber,^[111] and silicon,^[19,41] the different binding strength, strain effect, and electron conductivity still impact the nucleation and growth of VG. Therefore, selective growth on specific substrates becomes feasible for one-step fabrication. Chen and coworkers have successfully fabricated VG on patterned gold stripes.^[64] Experiments and simulations results showed that the electric field difference between gold stripes and unpattern SiO₂ influences the ion flux distribution, resulting in significant different growth rate of VG in different area of the substrate. Moreover, the substrate tempera-

Table 3. Parameters of growing VG in PECVD.

Plasma type	Precursor	Gas ratio [sccm]	Substrate type	Substrate temperature [°C]	Average growth rate [nm min ⁻¹]	Ref.
High-flux-ICP	CH ₄ /Ar	10:50	copper foil	<300	47	[68]
MW	CH ₄ /H ₂ /O ₂	10:50:0.5	graphite fiber	1377	17	[16]
DC glow	CH ₄ /Ar	150:1350	nickel foil	700	-	[113]
	(40%RH)					
MW	CH ₄ /CO ₂	1:2	nickel foil	400	101.7	[52]
ECR-MW	CH ₄ /Ar	5:25	Pt, Ni, Au, Cu, Si(100), Si(111), SiO ₂ and quartz	800	9 (max)	[109]
ECR-MW	CH ₄ /Ar	5:30	SiO ₂ /Si	800	67 (vertical)	[45]
ICP	C ₂ H ₂ /H ₂	2:1	glass	500	28	[72]
ICP	CH ₄ /H ₂	19:1	Si	680	50	[76]
MW	CH ₄ /Ar	1:8	Si	450	40	[116]
ICP	CH ₄ /H ₂	5:20	SiO ₂	900	2	[117]
ICP	C ₂ H ₂ /H ₂	4:1	Si	600	180	[50]
AEF-ICP	CH ₄ /methanol/ethanol	-	Si	650	52	[21]
CCP	CH ₄ /H ₂	40:20	soda-lime glass	580	6	[79]
ICP	CH ₄ /Ar/H ₂	50:21 000:900	Si	-	18 080	[19]
ICP	C ₂ H ₂ /H ₂	3:1	quartz	800	67 (max)	[74]
Helicon-ICP	CH ₄ /Ar	3:5	Si	300	260	[20]
ICP	methanol/chloroform	20:1	Si	650	192	[22]

ture also plays an important role in VG growth since it strongly affects the surface diffusion of carbon species.^[112] In RF-PECVD, external resistance heating is typically required to provide sufficient initial nucleation sites and promote crystallization, except in microwave-enhanced CVD where the plasma density is already high enough to enable VG growth at relatively low substrate temperatures.

Both the plasma type and the feedstock precursors have a significant impact on the properties of the plasma and the composition of radicals.^[17,20–22,74,113] Beside aforementioned plasma types in PECVD, the choice of gaseous or solid feedstock is also a critical parameter in controlling the growth of VG. Among carbon precursors, hydrocarbons are the most commonly used in PECVD systems. It has been reported that the C₂H₂ as a feedstock for VG growth results in a faster growth rate, well-vertically aligned, and a more uniform height distribution compared to CH₄, owing to the lower dissociation energy and higher density of carbon dimer (C₂) in C₂H₂.^[50,114] Besides, it has been found that CO,^[115] CO₂,^[52] and methanol^[22] can also be diluted with hydrocarbon sources to enhance the VG growth, owing to the etching effect of the generated H, OH, and O species on amorphous carbon.

Figure 8a demonstrates the successful production of ultrahigh vertical graphene with aligned orientation through an oxygen-assisted trimming (OAT) PECVD process.^[17] In this process, the height saturation stemming from the confluence of the VG flakes with prolonging the growth time was surmounted through eliminating the conjugated graphene flakes and amorphous carbon. Meanwhile, the oxygen functionalized VG flakes exhibited a branched structure, resulting in relatively uniform electric-field distribution and ion bombardment. Even after a growth time of 12 h, the growth rate was still maintained at a high value,

resulting in the final height of 80 μm (Figure 8b). The defects density of VG was also characterized using Raman spectroscopy. Figure 8c showed that the intensity ratios of D and G peaks derived from Raman spectra were higher for ultrahigh VG at the same growth time, owing to more branched edges compared to common VG. Interestingly, this ratio decreased as the growth time was prolonged, indicating the tunability of the defects structure (Figure 8c).

The vertical orientation of VG has demonstrated a beneficial structure for both ion and electron transportation in supercapacitors. As shown in Figure 8d, the ion diffusion direction of common rGO powder with polyvinylidene difluoride (PVDF) binder is uneven due to the presence of numerous micrometer-scale vacancies. Although horizontally stacked rGO films on collectors can serve as electrodes, this stacking arrangement still impedes the penetration of electrolyte ions. Meanwhile, the diffusion direction of electrolyte ions between rGO layers is perpendicular to the charge transfer direction of capacitors, leading to slow ion and charge transfer, thus not desirable for high charge/discharge rates. In stark contrast, vertically aligned rGO (VArGO) exhibited an open structure with ordered orientation. This homogeneous stacking and denser configuration facilitate fast ion/charge networks between rGO sheets, resulting in superior volumetric and areal electrochemical characteristics.^[24]

In addition to the vertical morphology of VG, the porosity, size of nanosheet, and density were also demonstrated to be controllable via introducing of nitrogen plasma in the fabrication of nitrogen doped vertical graphene (NVG) nanosheets.^[80] This resulted in a significant decrease in the distance between each nanosheet, gradually forming a continuously interconnected porous network in the NVG, as depicted in Figure 8e. Consequently, a tunable microstructure with a balanced

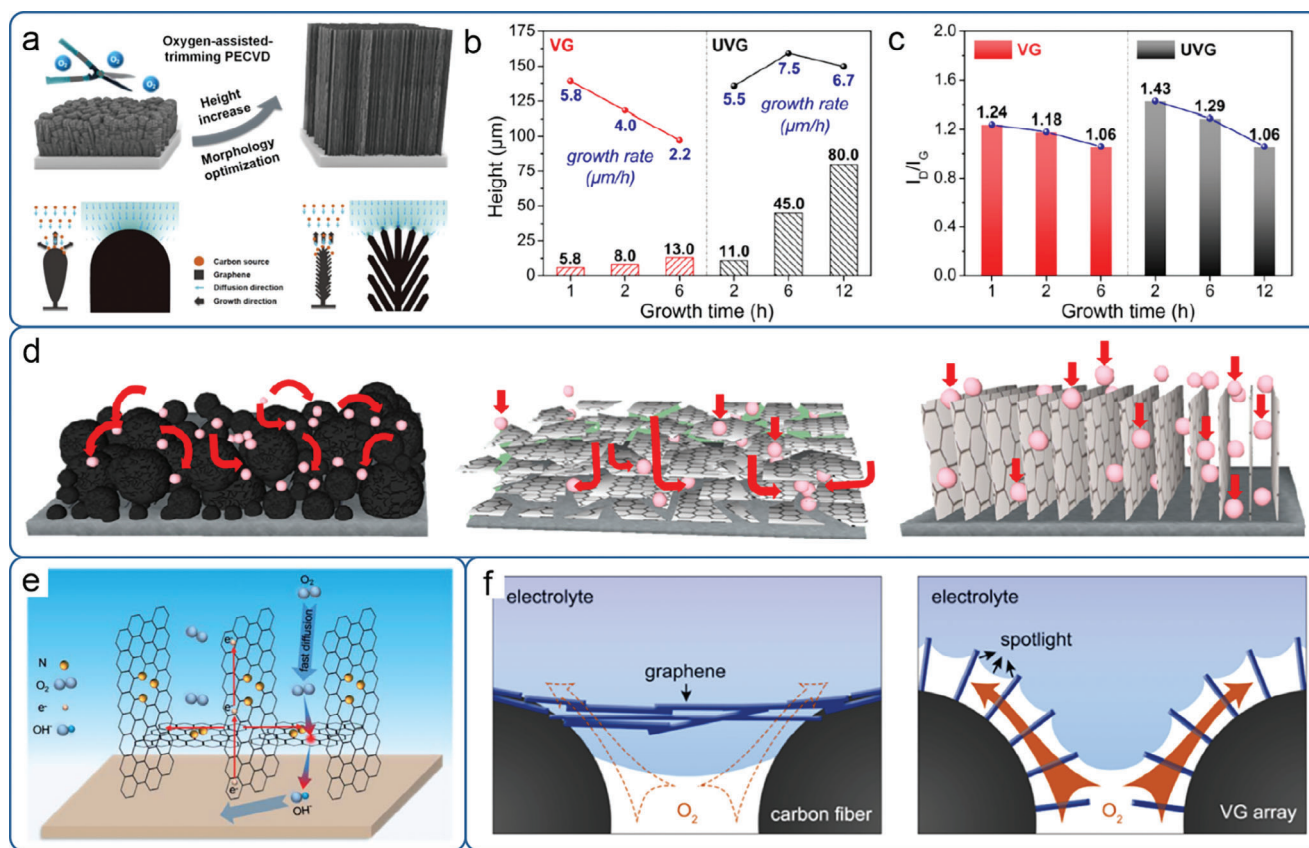


Figure 8. Morphology tailoring of VG. a) Schematic illustration of ultrahigh VG (UVG) fabricated in oxygen-assisted trimming PECVD. b) Height and growth rate of VG and UVG as a function of growth time. c) Intensity ratio of D peak to G peak of VG and UVG as a function of growth time. a–c) Reproduced with permission.^[17] Copyright 2021, American Chemical Society. d) Schematic illustrating ion diffusion based on rGO powder, rGO film, and VArGO. Reproduced with permission.^[24] Copyright 2014, American Chemical Society. e) Schematic showing the boost of electron and mass transfer in the interconnected nitrogen doped vertical graphene (NVG). Reproduced with permission.^[80] Copyright 2020, Royal Society of Chemistry. f) Schematic illustrating interface between disordered G electrode (left)/VG array (right) and electrolyte. Reproduced with permission.^[118] Copyright 2022, Elsevier.

micro/mesopores ratio was achieved, providing efficient electron and mass transfer pathways, thus contributing to fast kinetics during the ORR process. Besides, the tunable morphology of VG can also help construct solid-liquid-gas triple-phase boundary (TPB), where the electrolyte, electrode, reactant come to react in fuel cells, metal-air batteries, CO₂RR, NRR, photocatalysis.^[118] As shown in Figure 8f, electrodes coated with disordered graphene were found to be completely permeated by electrolyte, but the diffusion of O₂ through the electrolyte was hindered, resulting in insufficient gas supply at the electrode surface. On the other hand, VG array electrodes facilitated the formation of a real TPB architecture on each carbon fiber, enabling more desirable gas diffusion pathways due to the hydrophobic nature of VG. The solid VG surface could readily react with abundant O₂ from the gas/liquid phase while releasing oxygen intermediates in aqueous solutions, thus exposing sufficient active sites.

Generally, fabrication factors have a significant impact on the structure properties, including defects and morphological characteristics. The introduction of defects modifies the electronic structure and conductivity of the carbon matrix, providing ample active sites and achieving the desired intrinsic activity of VG. The morphological modulation strongly affects the electron/mass transfer capability, leading to enhanced reaction kinetics

of the whole electrochemical device.^[119] Therefore, structure engineering of VG via rational optimizing growing parameters is crucial in simultaneously controlling both defects and morphology of VG for the advancement of desirable applications in energy related field.

4. Energy Applications of VG

4.1. Supercapacitor

Supercapacitors are energy storage devices that rely on the charging and discharging processes at the interface of the electrode and electrolyte. A suitable supercapacitor electrode demands large surface area, low electrical/ionic resistance, ultra-fast dynamic response, and suitable scaffold for pseudocapacitive materials.^[86,120] VG is endowed with many unique characteristics such as large surface area, excellent electronic conductivity, robust mechanical property, which can significantly enhance the performance of capacitors. In electric double-layer capacitors (EDLC), VG can directly adsorb ions at the electrode/electrolyte interface, and in pseudocapacitors, it serves as a scaffold for loading electro-active materials.

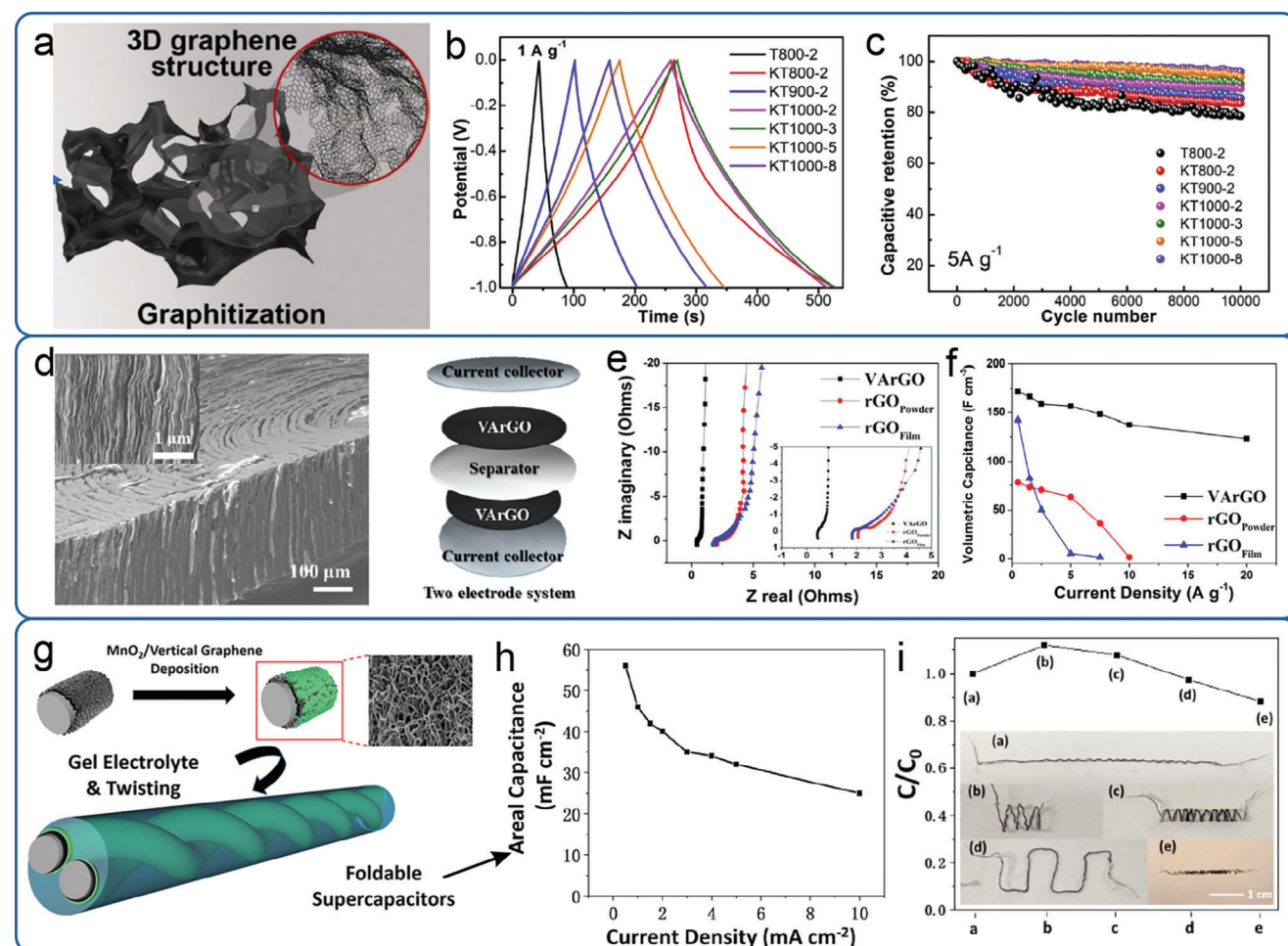


Figure 9. a) Schematic of 3D vertical graphene structure. b,c) The galvanostatic charge–discharge curves at current density of 1 A g⁻¹ and cycle performance of all samples at 5 A g⁻¹. a–c) Reproduced with permission.^[40] Copyright 2019, Elsevier. d) A SEM image of highly dense VarGO electrode and the VarGO based two electrode system without binder. e) Nyquist plots and f) rate performance of rGO film, rGO powder and VarGO. d–f) Reproduced with permission.^[24] Copyright 2014, American Chemical Society. g) Schematic showing the fabrication of foldable fiber-shaped supercapacitors. h) Areal capacitance of the fiber-shaped supercapacitors. i) Flexibility evaluation of the quasi-solid-state supercapacitors. g–i) Reproduced with permission.^[124] Copyright 2020, Elsevier.

The edge defects in VG play an important role in EDLC as they can directly influence the charge storage behavior.^[45,121] Previous studies have shown that VG fabricated in inductively coupled plasma enhanced CVD (ICPECVD), known as VGs-RF, and microwave plasma enhanced CVD (MPCVD), known as VGs-MW, possesses the same mass but different edge defect densities.^[82] VGs-RF exhibited 2.3 times larger mass specific capacitance and area specific capacitance compared to VGs-MW. Meanwhile, the vertical orientation and porous structure of VG also contribute to fast ion transportation in EDLC. A 3D network of VG structure was reported growing on Ni foam directly as the capacitor electrode through MPCVD.^[122] The straight-forward, open and porous structure of VG was proved to boost ion transportation, reduce low equivalent serial resistance, and resulting in a specific cell capacitance of 0.32 mF cm⁻² at 1 KHz and a relaxation constant time of 0.248 ms. Besides, high-temperature pyrolysis derived VG with hierarchical 3D structure was reported advantageous as an EDLC electrode.^[40] As shown in Figure

9a, alkaline-assisted one-step pyrolysis was conducted to convert waste tires into 3D VG after experiencing a multi-states morphology evolution. The optimized 3D VG electrode exhibited longer charge time and high areal capacitance. Moreover, it demonstrated excellent capacitive retention of up to 95.9%, attributed to the non-aggregation and high electrical conductivity features of the interlaced 3D graphene architecture (Figure 9b,c). Highly dense and vertically aligned reduced graphene oxide (VarGO) was also reported prepared in solution-based method as electrode materials in EDLC, shown in Figure 9d.^[24] The two-layer EDLC based on VarGO displayed the lowest charge transfer resistance of 0.44 Ω and a nearly vertical slope in the low-frequency region, indicating enhanced reaction kinetics due to the vertically aligned and exposed surface structure. Consequently, the volumetric capacitance of VarGO (171 ± 1 F cm⁻³) surpassed that of other samples. Even at high current density, VarGO demonstrated a high capacitance of 123 ± 1 F cm⁻³ (Figure 9e,f).

Supercapacitors with a high energy density can be achieved by anchoring active materials onto a conductive skeleton and induce fast reversible redox near the surface of electrodes.^[86] On this basis, VG can serve as an ideal skeleton for loading other active materials owing to its robust mechanical property and exposed surface structure. Recently, VG nanosheets loaded with MnO₂ on nickel wires were fabricated using a combination of PECVD and electrodeposition processes. Two such nickel wires were twisted and covered with a gel electrolyte, resulting in foldable supercapacitors (Figure 9g). The quasi-solid-state supercapacitor exhibits a remarkable areal capacitance up to 56 mF cm⁻² at a current density of 0.5 mA cm⁻² (Figure 9h). More importantly, it demonstrated impressive performance retention, with over 80% of its original performance preserved even in a deformed configuration (Figure 9i). This remarkable durability indicated significant potential for application in flexible and solid-state energy storage systems for electronic devices. Similarly, TiN nanoparticles were also reported deposited on VG to form TiN/VG electrodes for supercapacitors.^[123] The aqueous TiN/VG electrode can exhibit a high energy density of 6.1 μWh cm⁻² and high power density of 2718.4 μW cm⁻² at a voltage of 1.8 V. Even in fast scan rate, the optimal TiN/VG electrode can retain the capacitance at 89.5% after 10 000 cycles, showing superior structural stability for supercapacitors.

4.2. Rechargeable Battery

Lithium-ion batteries (LIBs) are the most popular commercialized rechargeable energy storage device,^[125] and extensive research has focused on developing reliable and safe electrode materials for electric vehicle and mobile device applications.^[126–129] However, practical implementation of high-energy components still poses challenges due to their low electrochemical kinetics and significant volume change during the lithiation and delithiation processes.^[130]

VG materials possess several appealing characteristics when used in LIBs. The vertical orientation of graphene sheets is parallel to the diffusion direction of Li ion, which could minimize the steric hindrance and improves reaction kinetics compared to other carbon materials like graphene powder, hard carbon, and carbon nanotubes.^[131] Meanwhile, VG possesses an exposed surface structure, high electronic conductivity and robust mechanical property, making it suitable as a matrix to load active species and as a coating layer on active materials. The physical properties could accommodate volume changes, besides, the sp² hybridization chemical property of VG surface slows electrochemical inertness to electrolyte and significantly slow down the formation of intermediate products in the solid electrolyte interphase (SEI) during the electrochemical process.^[132] For instance, VG nanowalls have been reported directly fabricated on copper foils using PECVD and acted as the anode in LIBs.^[133] This approach significantly increased the contact area between the electrolyte and active materials compared to carbon slurry-coated copper. Moreover, the nanocrystalline sp² C-C in VG suppressed the formation of undesirable SEI films during charge and discharge processes, leading to low charge transfer resistance according to electrochemical impedance spectroscopy (EIS) spectra. As a result, the VG electrode showed superior electrochemical proper-

ties with a high reversible discharge capacity of ≈190 mAh g⁻¹ at 3C, superior to ≈160 mAh g⁻¹ of commercial carbon slurry coated copper electrode. VG encapsulated porous Si@Ag particles (VG-PMSi@Ag) were also fabricated as the binder-free anode in LIBs, shown in Figure 10a.^[27] Enormous VG nanosheets grown on the surface of PMSi@Ag were constructed into a 3D conductive network, providing a fast lithium transfer pathway and alleviating large volume change of Si particles during cycling, therefore ensured the integration of the anode electrode (Figure 10b). Meanwhile, the VG coating layer also increased the active area of anode and prevented the direct contact between electrolyte and Si particles, thereby reducing the formation of unfavorable SEI at the interface. Consequently, the VG-PMSi@Ag showed a high reversible capacity of 1403.9 mAh g⁻¹ at 2.0 A g⁻¹ after 100 cycles and maintained a stable Coulombic efficiency compared to other electrodes (Figure 10c).

This unique structure of VG also benefit anode materials of sodium-ion batteries (SIBs), since it suffers from sluggish reaction kinetics and poor structure stability.^[134] Al₂O₃ coated nitrogen doped VG (NVG) on copper foils were fabricated using the HPECVD technique, followed by coating ultrathin amorphous Al₂O₃ film (≈1 nm) on the surface using the atomic layer deposition (ALD) method.^[135] The NVG/Al₂O₃ showed a vertically and closely connected morphology with nanosheets separated from each other. Moreover, the defective and porous structure of NVG was maintained even coated with an ultrathin Al₂O₃ layer, guaranteeing sufficient active sites for Na adsorption (Figure 10d). The successful coating of Al₂O₃ layer helped construct a beneficial 3D reactive interface region from the top to interior of VG electrodes, suppressing side reactions of electrolyte during cycling and providing unblocked ion transfer pathway (Figure 10e). As a result, the optimal NVG/Al₂O₃ electrode delivered a high reversible capacity of 835.0 mAh g⁻¹ at 0.1 A g⁻¹ (Figure 10f) and an excellent cycling stability (a retention of 92.3%) even after 5000 cycles. The advantages of VG are also evident when combined with other active materials. For example, wrinkled MoSe₂ nanosheets were sandwiched between a VG core and N-doped carbon shell through hydrothermal and polymerization (Figure 10g).^[136] This unique architecture showed high electrical conductivity, mechanical stability, and large porosity. The omnibearing conductive network facilitated fast electron transfer, leading to enhanced reaction kinetics. As a preliminary test, the sandwiched arrays electrode showed a high reversible capacity of 534.8 mAh g⁻¹ at 0.2 A g⁻¹, enhanced rate performance, and excellent long-term cycling stability (Figure 10h–j). Besides, the CoSe₂ loaded VG hierarchical architecture on carbon fiber cloth (CoSe₂@VG/CC) was also proposed via combined steps of PECVD, wet chemistry and thermal selenization.^[137] The 3D porous VG not only provide fast electron/mass transfer pathway, but also buffer the volume swelling and alleviate the agglomeration of CoSe₂ nanoparticles. As a result, the full cell comprising CoSe₂@VG/CC and active carbon cathode demonstrated a superior cyclic stability at 0.5 A g⁻¹ for 1800 cycles, showing high energy and power density of 116 and 7298 W kg⁻¹.

In this regard, VG materials with vertical orientation can readily serve as both supporting scaffolds and active materials for Na ion storage system. When utilized as a supporting scaffold, the morphological properties of VG strongly influence the reaction

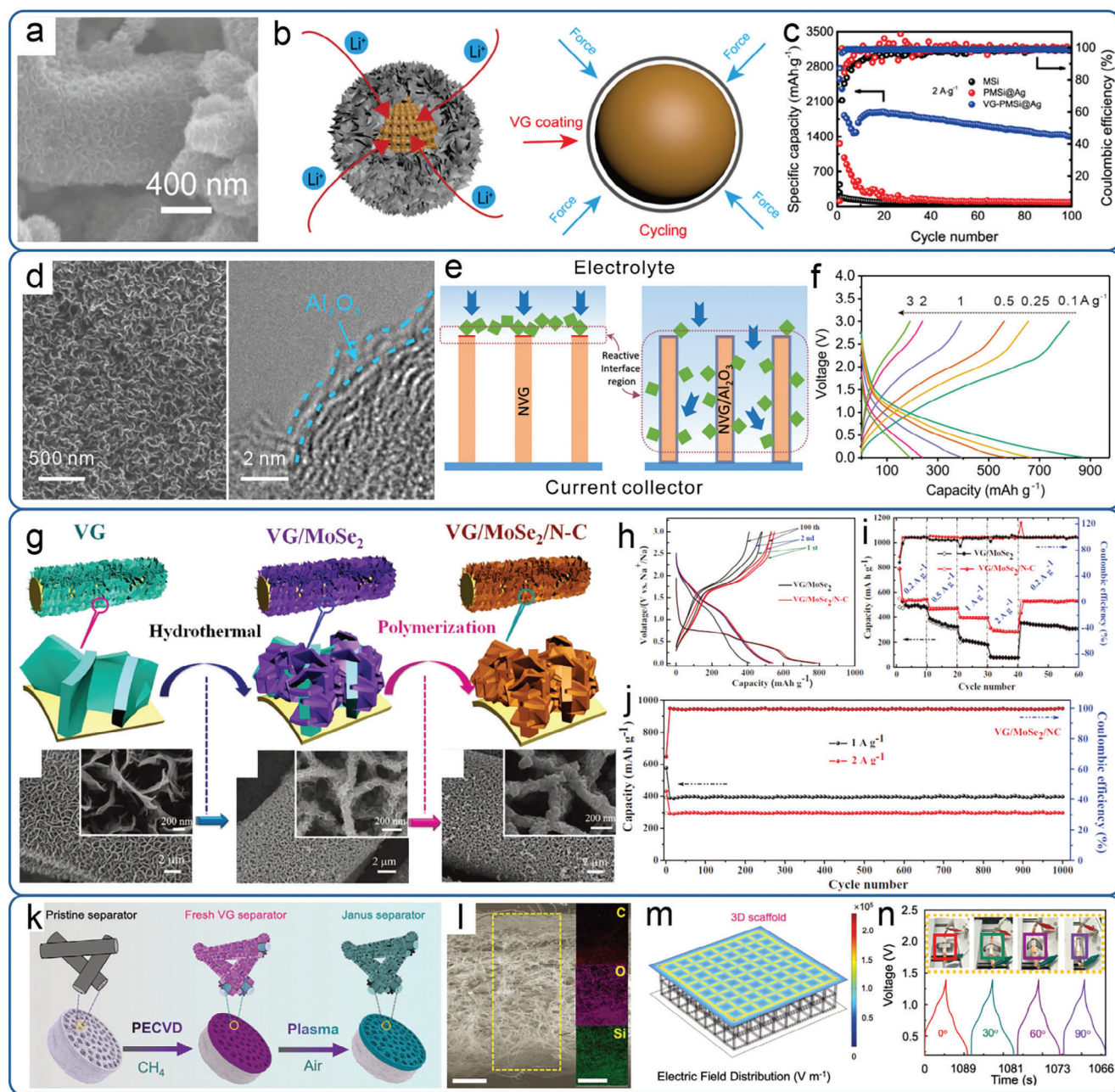


Figure 10. a) A SEM image of the VG-PMSi@Ag. b) Schematic illustration of the fast lithium-ion storage mechanism and alleviation of volume expansion of Si in VG-PMSi@Ag structure. c) Cyclic performance of three electrodes in 100 cycles. a–c) Reproduced with permission.^[27] Copyright 2022, American Chemical Society. d) SEM and TEM images of Al_2O_3 coated NVG electrode. e) Schematic illustration of enlarged reactive interface region after coating ultrathin Al_2O_3 compared with VG. f) Charge–discharge profiles of NVG electrode at the current density from 0.1 to 3 A g^{-1} . d–f) Reproduced with permission.^[135] Copyright 2021, Wiley-VCH. g) Schematic showing the fabrication of VG/MoSe₂/N-C as anode of sodium ion battery. h–j) Electrochemical characterizations of VG/MoSe₂ and VG/MoSe₂/N-C electrode. g–j) Reproduced with permission.^[136] Copyright 2016, Wiley-VCH. k) Schematic illustrating the fabrication of Janus separator (VG@glass fiber). l) Cross-section SEM image of Janus separator and the EDX elemental mapping of C, O, and Si. m) Electric field distribution of Janus separator structure. n) Flexibility evaluation of $\text{V}_2\text{O}_5//\text{Zn}$ battery using Janus separator. k–n) Reproduced with permission.^[139] Copyright 2020, Wiley-VCH.

kinetics due to their advantageous mass/electron transportation capabilities. The capacity contribution of VG is generally negligible, primarily attributed to its high graphitization and insufficient active sites. The none-doped VG with mainly sp^2 hybridized carbon atoms is electrochemically inert to reactants and the layer

separation for none-doped VG is insufficient for Na^+ motion. On the other hand, when used as active materials, it becomes necessary to modify the chemical structure of VG through heteroatom doping and pores/edges construction. Since the defect structure can readily alter the charge/spin distribution, construct

physical/chemical confinement and enlarging interlayer spacing, which can significantly boost the capacity of SIBs.^[13,138]

VG was also reported successfully used in the alkali metal batteries. As seen in Figure 10k, a Janus separator was fabricated via growing VG on one side of glass fiber with the other side pristine.^[139] It was discerned that the Janus separator showed porous and fibrous structure with VG spatially occupying near 30% of the total thickness, which is suitable for the Zn anode (Figure 10l). Finite element method was also employed to simulate local current density on VG side of Janus separator. It was found that such 3D VG scaffold could introduce a uniformly distributed electric field, enabling even deposition of Zn on the VG side. This effectively suppressed dendritic growth and minimized the formation of by-products (Figure 10m). Moreover, the VG-coated Janus separators demonstrated high electrochemical stability under deformations when used in flexible Zn-ion batteries (Figure 10n). The uniform electrical field construction was also employed in Na and Li metal battery.^[140–143] A flexible CC harnessing VG and Co nanoparticle/N-doped carbon decorator (Co-VG/CC) was reported as an ideal host for molten Na infusion.^[140] In this configuration, the VG was demonstrated to enhance the overall conductivity, alleviate electrical field concentration, and accommodate volume change of Na anode. As a result, the symmetric cell realized a high capacity of 6.0 mAh cm⁻² for 1000 h and exhibited a high lifespan of 2000 h. Similarly, a 3D conductive multichannel carbon framework with homogeneously distributed VG (VGWs@MCF) was constructed in both Li|VGWs@MCF anode and LFP|VGWs@MCF (NCM₈₁₁|VGWs@MCF) cathode.^[141] The presence of VG facilitated rapid, continuous, and smooth electron transfer channels, resulting in uniform interfacial Li ion migration within the anode and improved Li ion transfer kinetics, particularly at high current densities.

4.3. Oxygen Electrocatalyst

With the rapid increase in energy demands and the growing concern for environmental issues, the development of clean energy is of vital importance to manifest large scale and affordable energy supply in an environmentally benign way. Several energy conversion devices, such as fuel cells, metal-air batteries, and water electrolysis, have been identified as promising solutions.^[144–147] However, their widespread application is still impeded by inherently sluggish ORR and OER, mainly due to the complex proton-coupled electron transfer processes.^[148] Therefore, the search for high-efficiency catalysts that minimize overpotential and maximize current density have always been the key goal.

Bare VG have been reported selectively reduce O₂ to produce H₂O₂ at high current density (>100 mA cm⁻²) in the absence of transition metals, which outperformed most catalysts reported to date for electrochemical produce of H₂O₂.^[118] The remarkable performance was attributed to the abundance of active sites on the edges of VG and the rapid electron transfer during the ORR process. Additionally, the intrinsic hydrophobicity of VG helps to construct a beneficial solid–liquid–gas interface that can both rapidly supply sufficient O₂ and high utilization of active sites in a flow cell. Moreover, heteroatoms-doped VG nanosheets have

demonstrated suitable bonding strength with oxygen intermediates and possess an advantageous morphological architecture, resulting in high intrinsic catalytic activity and excellent mass transfer capability.^[80,96]

Nitrogen doping is the most popular method to alter the charge/spin distribution, leading to the modification of electronic of the adjacent carbon atoms.^[94] Metal-free nitrogen-doped carbon nanowall electrodes were first fabricated using a two-step process via PECVD on glassy carbon substrates.^[102] Raman spectroscopy revealed that the nitrogen doping could increase defects density via bonding carbon atoms with pyridinic, pyrrolic, and quaternary nitrogen. XPS measurements showed that the atomic content of nitrogen ranged from 4% to 20% depending on the doping parameters. Afterward, one-step fabrication of nitrogen doped VG (NVG) was achieved using HPECVD.^[80] Nitrogen plasma was introduced during the growing of VG, resulting in morphological and chemical structure changes with varying nitrogen doping levels. Electrochemical tests demonstrated that the optimized NVG catalyst displayed a more positive onset value and higher diffusion limiting current density compared to non-doped VG, although it slightly lagged behind the commercial benchmark Pt/C catalyst. This superior performance can be attributed to the synergistic effect of well-balanced meso-/microporosity and an interconnected, vertically arranged structure. Besides, NVG can be used as cathode catalyst in Zn-air batteries showing excellent discharge performance with high energy density, which outperformed commercial Pt/C. Although the electrocatalytic activity of these catalysts could be tuned by nitrogen doping, they were not yet suitable for practical use in real devices due to several factors such as suboptimal doping level, insufficient active sites, limited electron transfer, and poor stability under harsh conditions.

Beyond single doping, nitrogen, and oxygen co-doped VG (VGNO) have also been demonstrated as effective oxygen electrocatalyst. The fabricated VGNO showed a preferred vertical orientation with a high growth rate and mass yield, as depicted in Figure 11a. The introduction of nitrogen and oxygen plasma successfully regulated the plasma radicals, including C₂, CN, and O, which play crucial roles in governing bonding state of graphene structure. This resulted in a high doping content of nitrogen and oxygen, along with a highly defective structure. The VGNO catalyst showed a ORR-OER bifunctional electrochemical activity with a low potential gap of 0.89 V between the OER acquired at 10 mA cm⁻² and the half-wave potential of ORR (Figure 11b). The enhanced reaction kinetics was verified by EIS, confirming a superior charge transfer process in VGNO (Figure 11c). More importantly, the VGNO catalyst showed an excellent long-term galvanostatic charge/discharge performance in both aqueous and solid-state rechargeable Zn-air batteries. This outstanding performance could be attributed to the vertical oriented morphology and preferable doping configuration of VGNO, which offered abundant active sites on the accessible surface and appropriate bonding strength with oxygen intermediates (Figure 11d,e).

Oxygen functionalization is a conventional method used to enhance the catalytic activity of VG catalysts, typically for OER in alkaline and acidic electrolyte, since the edge-rich structure is easily to be functionalized by directly exposed in the air and electrochemical treatment (Figure 11f). Surface functionalization introduces oxygen-containing functional groups (such as C=O

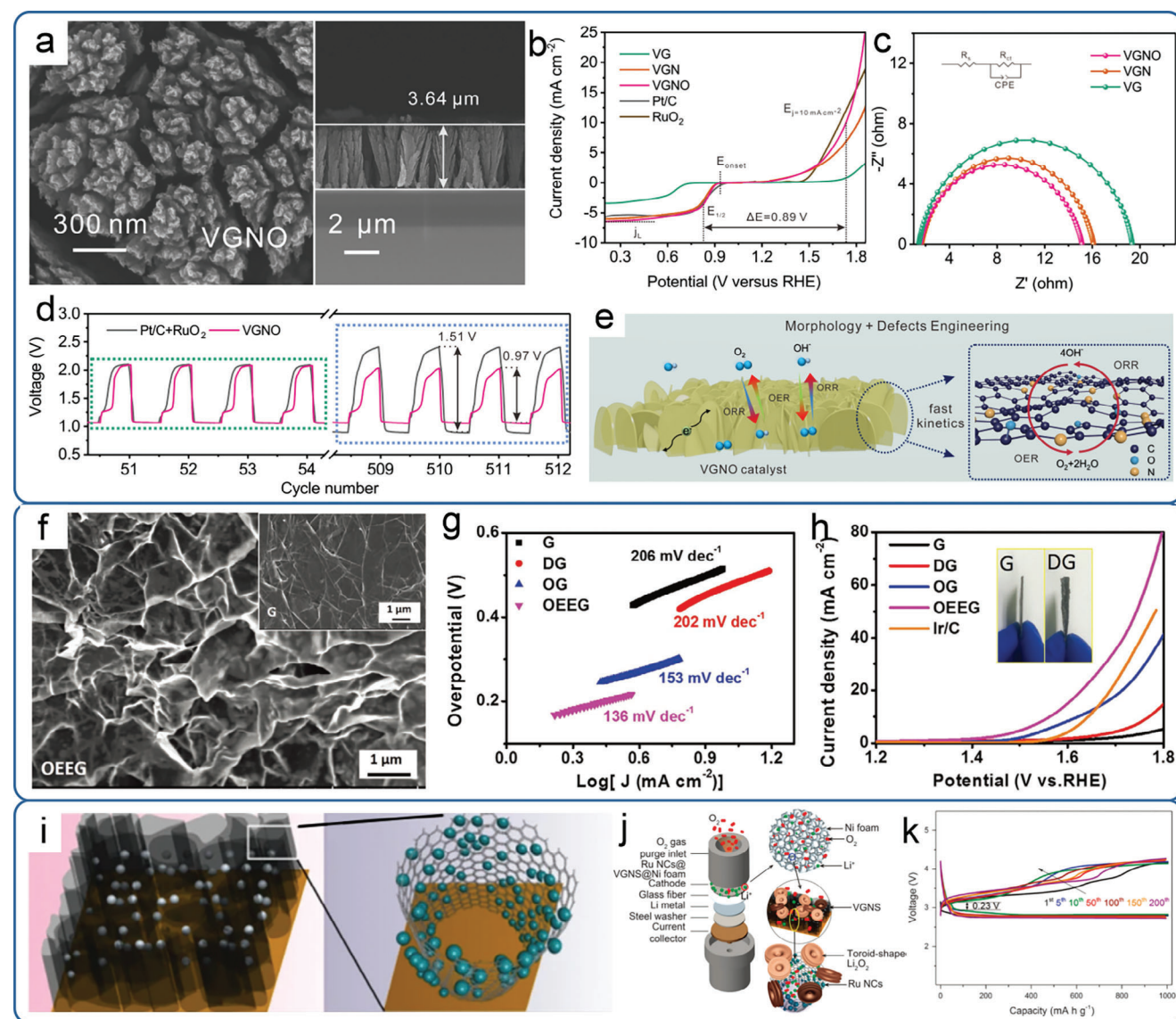


Figure 11. a) SEM images of nitrogen and oxygen co-doped VG catalyst. b) Polarization curves of various catalysts for ORR and OER. c) Nyquist plots of various catalysts. The inset is the equivalent circuit. d) Galvanostatic charge–discharge performance of VGNO based aqueous Zn–Air battery with commercial Pt/C+RuO₂ for comparison. e) Schematic illustrating the mechanism of enhanced performance for ORR and OER of VGNO catalyst. a–e) Reproduced under terms of the CC-BY license.^[49] Copyright 2022, Wiley-VCH. f) SEM image of vertically oriented electrochemically exfoliated graphene (OEEG) nanosheets array catalyst. The inset is a typical SEM image of pristine graphite. g) Tafel slopes and h) polarization curves of various catalysts. f–h) Reproduced with permission.^[149] Copyright 2020, Wiley-VCH. Schematic illustrating the i) structure of Ru decorated VGNs and j) Ru decorated VGNs on Ni foam as cathode in Li–O₂ cell. k) Charge–discharge profiles of Ru decorated VGNs electrode at a current density of 200 mA g^{−1}. i–k) Reproduced under terms of the CC-BY license.^[108] Copyright 2016, Nature Publishing Group.

and COOH species), which alter the charge distribution of nearby carbon atoms and improve the reaction kinetics of the OER (Figure 11g).^[96,149] The oxygen-functionalized VG catalyst demonstrated superior OER performance to undoped counterparts and the overpotential can be reduced to 334 mV at 10 mA cm^{−2} in 0.5 M H₂SO₄ solutions (Figure 11h).

On the other hand, VG decorated with platinum group metals (PGM) is indeed a feasible method to enhance oxygen electrocatalytic performance, since the open structure with abundant defects can alter the coordination environment and surrounding electronic structure. This modification facilitates an enhanced

charge-transfer mechanism, which in turn enhances and stabilizes PGM nanoparticles on the VG surface.^[150] It was reported that Ru decorated VG@Ni foam was fabricated first by growing VG on the Ni foam via PECVD technique, and followed by loading Ru on VG via a typical pyrolysis method (Figure 11i).^[108] The Ru decorated VG@Ni foam was directly used as the cathode in an Li–O₂ cell without the introduction of any binder (Figure 11j). In this architecture, the reaction kinetics of ORR and OER were accelerated due to the sufficient active sites and accessible transfer pathway for O₂. As a result, the assembled Li–O₂ cell showed a low charge overpotential (≈0.45 V) and high reversible

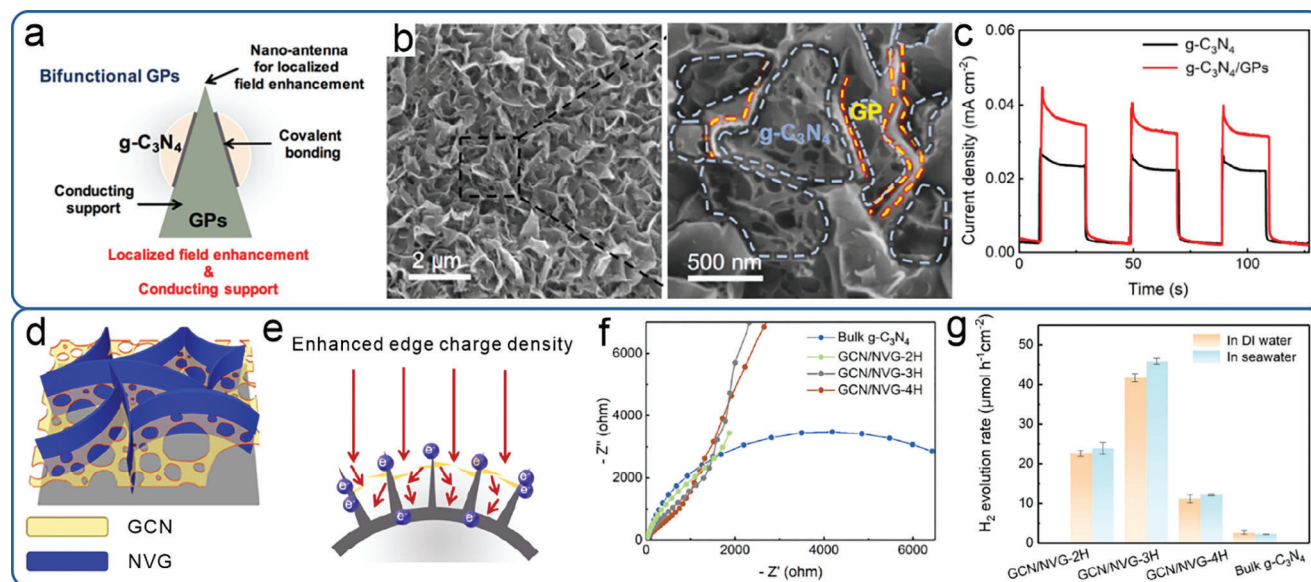


Figure 12. a) Schematic showing graphene petals both as localized field enhancement material and conducting support in heterostructure. b) SEM images of g-C₃N₄/GP structure. c) Performance of g-C₃N₄/GP structure in photocatalytic hydrogen evolution. a–c) Reproduced with permission.^[152] Copyright 2020, Elsevier. d) Schematic of hybrid GCN/NVG structure. e) Photo and electron management of GCN/NVG for photocatalyst. f) Nyquist plots and g) photocatalytic H₂ evolution rate of various catalysts. d–g) Reproduced with permission.^[87] Copyright 2020, Elsevier.

capacity (23 864 mAh g⁻¹) at high current density (200 mA g⁻¹) (Figure 11k).

4.4. Photocatalyst

Solar energy is the most abundant and viable energy source, making it well-suited for meeting our ever-growing energy needs. One promising application of solar energy is photocatalytic water splitting, which produces hydrogen gas in a clean and cost-effective manner, thereby revolutionizing our energy systems.^[151] Typically, photocatalytic systems consist of a conductive support, a semiconducting photocatalyst and noble metal nanoparticles. Among these components, the presence of noble metal nanoparticles plays a crucial role in enhancing catalytic activity due to the strong localized electric field enhancement. VG is composed of tapered and ultrathin edges, which can accumulate electrons at the tip of VG nanosheets, as shown in Figure 12a. After covalent bonding with photocatalysts, the VG nanosheets not only can serve as a conducting support, but also a nano-antenna for localized field enhancement. The unique surface morphology of the g-C₃N₄/VG showed that the g-C₃N₄ networks were seamlessly integrated with the basal region of VG nanosheets and leave the exposed tips region, which was demonstrated to give an enhanced interaction with light (Figure 12b). Consequently, the average photocurrent of the g-C₃N₄/VG is much higher than that of g-C₃N₄, showing the capability of VG to enhance charge generation and charge transfer efficiency (Figure 12c). Nitrogen doped VG was also shown efficient to form heterojunctions with g-C₃N₄ through a space-confined synthesis strategy, as shown in Figure 12d. In this structure, nitrogen doping was demonstrated showing a n-type doping behavior, allowing additional electrons to be donated to the graphene structure, making it

highly-desirable for photocatalytic processes (Figure 12e). This was confirmed by the EIS measurement, suggesting the reduced interfacial charge-transfer resistance and enhanced the transmit of electron–hole pairs (Figure 12f). Subsequently, the hybrid g-C₃N₄/NVG exhibited a high areal H₂ evolution rate of 41.7 and 45.8 μmol h⁻¹ cm⁻² in DI water and simulated seawater, respectively (Figure 12g).

4.5. Vanadium Redox Flow Battery

Furthermore, the vanadium redox flow battery (VRFB) is also an ideal energy storage solution for loading shift in power grid as well as in energy conversion system.^[153] To improve the electrochemical activity of electrodes, it is crucial to increase the surface area and number of active sites. The highly open structure and extended edges of VG were expected to enhance electrochemical activity, making it suitable for practical use in VRFBs.^[154] 3D VG decorated carbon felts were reported synthesized using MPCVD, and were directly used as a positive electrode in VRFBs.^[155] Following the MPCVD process, the carbon felts were wrapped by VG with the controllable diameter. Meanwhile, the surface area, electric resistance, and the defects density can be easily controlled by the ratio of reactant and deposition time. The full exposure of graphene edges with good catalytic activities to the vanadium ions can boost reaction rate of the vanadium ions. Besides, the arrangement of vertical graphene nanosheets provides unblocked mass transfer channels and guarantee fast electron transportation. As a result, this unique composite electrode showed enhanced electrochemical activity toward VO₂⁺/VO²⁺ redox reactions, thereby enhancing energy efficiency and demonstrating exceptional charge-discharge performance, even after 200 cycles.

5. Conclusion and Outlooks

In the pursuit of achieving better electrode reaction kinetics and enhanced structure stability in electrochemical performance, vertically oriented graphene nanosheets have emerged as a highly promising candidate compared to other materials such as carbon nanodots, CNTs, randomly distributed graphene, and graphene-like powder. In this review, the fabrication routines of VG have been shed light upon, which can be largely divided into solution-based and vacuum based methods. The unique advantages and current issues of each synthesis methods are presented in **Table 1**. VG exhibits a unique structure with the preservation of its intrinsic physical and chemical properties of 2D graphene and vertically aligned architecture. In general, VG possesses all merits of 2D graphene, including high thermal/electrical conductivity, large surface area, high machinal strength, and facile functionalization. Furthermore, VG with well oriented graphene nanosheets have beneficial architecture for both ion and charge transport, as well as for anchoring and stabilizing active materials. Additionally, the presence of significant edge defects in VG alters the surface charge distribution and spin density, further enhancing its performance. Considering these factors, strenuous efforts should be made on the following aspects:

5.1. Graphitization Control

Solution-based method is a simple and low-cost approach for VG growth based on graphene-like powders or chemically reduced graphene oxide. However, the fabrication always requires organic materials or reduced graphene oxide through pyrolysis, template-based formation, hand-rolling and cutting, and self-assembly. The inherently low graphitization hinders the fully tuning of doped states and conductivities to ions and electrons. Although high temperature is beneficial for carbonization of organics and reduction of GO, the long-time treatment could inevitably cause weight loss or structure destruction. Therefore, it is suggested to investigate feasible routine to enhance the crystallization using directional heating for the full use of 2D electronic properties for solution-based method. Taking the advantages of vacuum-based approaches, PECVD offers intrinsic versatilities in terms of growing parameters to modulate the chemical/physical properties. The vertical morphology, defect structure and graphitization degree are both important for mass/electron transportation. Nevertheless, it is the key point to illuminate the structure-preparation relationships for rational design of the vertical graphene and propose an indicator to balance the graphitization, defect density, vertical orientation targeting energy conversion and storage applications.

5.2. Doping Implementation

The unique structure of VG enhances reaction kinetics, which strongly correlates with the vertical morphology, surface active sites, electron transport properties. However, most existing research has primarily focused on pristine VG or VG-based hybrids, exploring aspects such as height, vertical orientation, and related morphological features, while paying less attention to defects control, specifically heteroatom doping of VG. Heteroatom

doping can significantly modify the electronic structure, chemical reactivity, and physical properties of VG. It can introduce localized states within the energy bandgap, thereby tuning the electrical conductivity and creating active sites for electrochemical reactions. The presence of heteroatoms can create new chemical bonds and alter the interlayer interactions, resulting in modifications to the vertical stacking behavior of graphene layers. Nonetheless, it is still lacking in the fully understanding of the mechanism of doping process in one-step or multi-step process especially in plasma-based method, due to the complexity of plasma environment. In this sense, *operando* inspection during doping process is highly desired to obtain critical parameters for the tuning of kinetics and thermodynamics. Overall, it is imperative to dedicate more effort to unraveling the relationship between doping processes and the atomic-scale structure of VG to meet both physical and chemical properties in real devices, aiming to propose a feasible methodology to guide rational design of heteroatom-doped structure.

5.3. Device Applications

Although VG has been applied in different energy conversion and storage system as active materials, modifiers, and scaffolds. A comprehensive understanding of the underlying mechanisms responsible for enhancing the electrochemical performance of practical devices has not been reached. Therefore, the development of suitable electrochemical models and advanced in situ characterization techniques is imperative for elucidating the intricate electrochemical behavior exhibited by VG-based devices. Furthermore, it is essential to carefully evaluate pragmatic parameters such as Coulombic efficiency, mass/area loading, temperature, and the partial pressure or concentration of reactants, as they exert vital influence on the overall electrochemical performance. These endeavors are crucial for further advancing VG-based devices and optimizing their practical applications.

5.4. Large-Scale Synthesis

Additionally, more endeavors are encouraged to propose new fabrication techniques, which are capable of mass production with high growth rate, minimum processing cost, and reduce complexity to realize the commercial value of the VG for large-scale energy applications. On this basis, the one-step fabrication and doping strategy is highly desired to attain high uniformity and low impurities, typically for heteroatom-doped VG. The plasma-based technique is a feasible method with controllable morphology and chemical structure. However, it faces challenges due to its low growth rate and the requirement of a harsh vacuum environment. This restricts its widespread application, especially considering that many materials struggle to maintain their structural integrity at high temperatures and low pressures. To address these issues, developing advanced setup constructions with high plasma density is a promising approach. By increasing the plasma density, the growing substrate temperature can be reduced, making it easier to retain the structural stability of sensitive materials and reduce energy consumption. Additionally, a higher plasma density helps alleviate edge saturation, resulting

in a better compatibility of VG with other materials and an increased growth rate. By optimizing the plasma density in the fabrication process, it is expected to bridge the existing gap between lab-scale synthesis and industrial production.

In summation, although there is still missing gaps in exploring the advances in material synthesis and structural investigation, it is still highly worthy to make even greater efforts to overcome these deficiencies. Overall, numerous research have been devoted to studying the VG in energy-related applications. We believe that through continuous studies on the morphology and defects engineering, highly crystalline VG with effective doping will have ever greater potential to be commercialized in large-scale, and as well as flexible all-solid-state, for advanced energy storage and conversion devices. We hope that this review can offer a comprehensive basis for rational structure design of VG-based composites, thus facilitating the advancement of electrode materials in various energy and environmental applications.

Acknowledgements

The work is supported by the National Natural Science Foundation of China (51602290), the Key R&D and Promotion Project of Henan Province (212102210600), and the National Natural Science Foundation of Henan Province (222300420546).

Conflict of Interest

The authors declare no conflict of interest.

Keywords

controllable synthesis, energy applications, structure engineering, vertical graphene

Received: September 10, 2023

Revised: October 17, 2023

Published online:

- [1] S. Chu, A. Majumdar, *Nature* **2012**, 488, 294.
- [2] H. Jin, C. Guo, X. Liu, J. Liu, A. Vasileff, Y. Jiao, Y. Zheng, S.-Z. Qiao, *Chem. Rev.* **2018**, 118, 6337.
- [3] Y. Li, Y. Lu, P. Adelhelm, M.-M. Titirici, Y.-S. Hu, *Chem. Soc. Rev.* **2019**, 48, 4655.
- [4] X. Meng, X. Deng, L. Zhou, B. Hu, W. Tan, W. Zhou, M. Liu, Z. Shao, *Energy Environ. Mater.* **2021**, 4, 126.
- [5] S. Dou, L. Tao, R. Wang, S. El Hankari, R. Chen, S. Wang, *Adv. Mater.* **2018**, 30, 1705850.
- [6] L. Zu, W. Zhang, L. Qu, L. Liu, W. Li, A. Yu, D. Zhao, *Adv. Energy Mater.* **2020**, 10, 2002152.
- [7] R. Raccichini, A. Varzi, S. Passerini, B. Scrosati, *Nat. Mater.* **2015**, 14, 271.
- [8] F. Bonaccorso, L. Colombo, G. Yu, M. Stoller, V. Tozzini, A. C. Ferrari, R. S. Ruoff, V. Pellegrini, *Science* **2015**, 347, 1246501.
- [9] Q. Zhang, C. Wang, Z. Xie, Z. Zhou, *Energy Environ. Mater.* **2022**, 5, 1103.
- [10] Z. Zhang, C.-S. Lee, W. Zhang, *Adv. Energy Mater.* **2017**, 7, 1700678.
- [11] C. Tang, Q. Zhang, *Adv. Mater.* **2017**, 29, 1604103.
- [12] J. Han, I. Johnson, M. Chen, *Adv. Mater.* **2022**, 34, 2108750.

- [13] J. Xu, M. Wang, N. P. Wickramaratne, M. Jaroniec, S. Dou, L. Dai, *Adv. Mater.* **2015**, 27, 2042.
- [14] Y. Lu, Y. Lu, Z. Niu, J. Chen, *Adv. Energy Mater.* **2018**, 8, 1702469.
- [15] Z. Bo, Y. Yang, J. Chen, K. Yu, J. Yan, K. Cen, *Nanoscale* **2013**, 5, 5180.
- [16] T. Bhuvana, A. Kumar, A. Sood, R. H. Gerzeski, J. Hu, V. S. Bhadram, C. Narayana, T. S. Fisher, *ACS Appl. Mater. Interfaces* **2010**, 2, 644.
- [17] J. Han, Y. Ma, M. Wang, L. Li, Z. Tong, L. Xiao, S. Jia, X. Chen, *ACS Appl. Mater. Interfaces* **2021**, 13, 12400.
- [18] X. Song, J. Liu, L. Yu, J. Yang, L. Fang, H. Shi, C. Du, D. Wei, *Mater. Lett.* **2014**, 137, 25.
- [19] H. Zhang, S. Wu, Z. Lu, X. Chen, Q. Chen, P. Gao, T. Yu, Z. Peng, J. Ye, *Carbon* **2019**, 147, 341.
- [20] P. Ji, J. Chen, T. Huang, C. Jin, L. Zhuge, X. Wu, *Diam. Relat. Mater.* **2020**, 108, 107958.
- [21] S. Xu, S. Wang, Z. Chen, Y. Sun, Z. Gao, H. Zhang, J. Zhang, *Adv. Funct. Mater.* **2020**, 30, 2003302.
- [22] S. Xu, T. Cheng, Q. Yan, C. Shen, Y. Yu, C.-T. Lin, F. Ding, J. Zhang, *Adv. Sci.* **2022**, 9, 2200737.
- [23] H. Ci, H. Chang, R. Wang, T. Wei, Y. Wang, Z. Chen, Y. Sun, Z. Dou, Z. Liu, J. Li, P. Gao, Z. Liu, *Adv. Mater.* **2019**, 31, 1901624.
- [24] Y. Yoon, K. Lee, S. Kwon, S. Seo, H. Yoo, S. Kim, Y. Shin, Y. Park, D. Kim, J.-Y. Choi, H. Lee, *ACS Nano* **2014**, 8, 4580.
- [25] W. Li, X. Li, W. Chang, J. Wu, P. Liu, J. Wang, X. Yao, Z.-Z. Yu, *Nano Res.* **2020**, 13, 3048.
- [26] L. Jiang, T. Yang, F. Liu, J. Dong, Z. Yao, C. Shen, S. Deng, N. Xu, Y. Liu, H.-J. Gao, *Adv. Mater.* **2013**, 25, 250.
- [27] Y. Mo, S. Li, J. Yu, *ACS Appl. Nano Mater.* **2022**, 5, 8205.
- [28] X. Kong, G. Liu, S. Tian, S. Bu, Q. Gao, B. Liu, C.-S. Lee, P. Wang, W. Zhang, *Small* **2022**, 18, 2204615.
- [29] Z. Shi, H. Ci, X. Yang, Z. Liu, J. Sun, *ACS Nano* **2022**, 16, 11646.
- [30] A. Vesel, R. Zaplotnik, G. Primc, M. Mozetic, *Materials* **2019**, 12, 2968.
- [31] N. M. Santhosh, G. Filipič, E. Tatarova, O. Baranov, H. Kondo, M. Sekine, M. Hori, K. (K.) Ostrikov, U. Cvelbar, *Micromachines* **2018**, 9, 565.
- [32] W. Zheng, X. Zhao, W. Fu, *ACS Appl. Mater. Interfaces* **2021**, 13, 9561.
- [33] S. Xu, J. Zhang, *Small Struct.* **2020**, 1, 2000034.
- [34] K. Chi, X. Zhang, X. Tian, Z. Zhang, Z. Wu, F. Xiao, S. Wang, *ChemElectroChem* **2020**, 7, 406.
- [35] X. Guo, Y. Li, Y. Ding, Q. Chen, J. Li, *Mater. Des.* **2019**, 162, 293.
- [36] F. An, X. Li, P. Min, H. Li, Z. Dai, Z.-Z. Yu, *Carbon* **2018**, 126, 119.
- [37] F. An, X. Li, P. Min, P. Liu, Z.-G. Jiang, Z.-Z. Yu, *ACS Appl. Mater. Interfaces* **2018**, 10, 17383.
- [38] J. H. Kim, J. M. Kim, G. W. Lee, G. H. Shim, S. T. Lim, K. M. Kim, T. T. Nguyen Vo, B. Kweon, S. Wongwises, D. W. Jerng, M. H. Kim, H. S. Ahn, *ACS Nano* **2021**, 15, 2839.
- [39] M. Sun, Y. Chen, L. Fan, M. Wu, C. Yang, *J. Mater. Sci. Mater. Electron.* **2022**, 33, 10919.
- [40] C. Wang, D. Li, T. Zhai, H. Wang, Q. Sun, H. Li, *Energy Storage Mater.* **2019**, 23, 499.
- [41] H. Wang, E. Gao, P. Liu, D. Zhou, D. Geng, X. Xue, L. Wang, K. Jiang, Z. Xu, G. Yu, *Carbon* **2017**, 121, 1.
- [42] D. Han, Y.-H. Zhao, Y.-F. Zhang, S.-L. Bai, *RSC Adv.* **2015**, 5, 94426.
- [43] Y.-F. Zhang, D. Han, Y.-H. Zhao, S.-L. Bai, *Carbon* **2016**, 109, 552.
- [44] F. Guo, A. Mukhopadhyay, B. W. Sheldon, R. H. Hurt, *Adv. Mater.* **2011**, 23, 508.
- [45] S. Ghosh, S. R. Polaki, M. Kamruddin, S. M. Jeong, K. (K.) Ostrikov, *J. Phys. Appl. Phys.* **2018**, 51, 145303.
- [46] H. Zheng, Q. Chu, P. Zheng, L. Zheng, X. Zheng, L. Shao, F. Wu, Z. Wu, Y. Jiang, Y. Zhang, *J. Phys. Chem. C* **2020**, 124, 21684.
- [47] Y. Li, C. Ai, S. Deng, Y. Wang, X. Tong, X. Wang, X. Xia, J. Tu, *Mater. Res. Bull.* **2021**, 134, 111094.
- [48] C. Shen, S. Xu, Z. Chen, N. Ji, J. Yang, J. Zhang, *Small* **2023**, 19, 2207745.

- [49] Z. Wu, Y. Yu, G. Zhang, Y. Zhang, R. Guo, L. Li, Y. Zhao, Z. Wang, Y. Shen, G. Shao, *Adv. Sci.* **2022**, 13, 2200614.
- [50] M. Y. Zhu, R. A. Outlaw, M. Bagge-Hansen, H. J. Chen, D. M. Manos, *Carbon* **2011**, 49, 2526.
- [51] M. Cai, R. A. Outlaw, R. A. Quinlan, D. Premathilake, S. M. Butler, J. R. Miller, *ACS Nano* **2014**, 8, 5873.
- [52] M. Su, H. Yang, Z. Liu, E. Wu, X. Chen, Z. Bo, L. Dai, K. (K.) Ostrikov, *Carbon* **2022**, 197, 301.
- [53] Y. Ando, X. Zhao, M. Ohkohchi, *Carbon* **1997**, 35, 153.
- [54] Y. Wu, P. Qiao, T. Chong, Z. Shen, *Adv. Mater.* **2002**, 14, 64.
- [55] Á. B. Murcia, J. Geng, *J. Nanosci. Nanotechnol.* **2013**, 13, 5849.
- [56] A. Roy, D. Das, *Diam. Relat. Mater.* **2018**, 88, 204.
- [57] D. A. Boyd, W.-H. Lin, C.-C. Hsu, M. L. Teague, C.-C. Chen, Y.-Y. Lo, W.-Y. Chan, W.-B. Su, T.-C. Cheng, C.-S. Chang, C.-I. Wu, N.-C. Yeh, *Nat. Commun.* **2015**, 6, 6620.
- [58] A. Kumar, A. A. Voevodin, D. Zemlyanov, D. N. Zakharov, T. S. Fisher, *Carbon* **2012**, 50, 1546.
- [59] Z. Wang, H. Ogata, S. Morimoto, M. Fujishige, K. Takeuchi, Y. Hashimoto, M. Endo, *Carbon* **2014**, 72, 421.
- [60] Z. Bo, M. Su, H. Yang, S. Yang, J. Yan, K. Cen, *Rev. Sci. Instrum.* **2020**, 91, 076105.
- [61] J. Hopwood, *Plasma Sources Sci. Technol.* **1992**, 1, 109.
- [62] M. Zhu, J. Wang, R. A. Outlaw, K. Hou, D. M. Manos, B. C. Holloway, *Diam. Relat. Mater.* **2007**, 16, 196.
- [63] R. Roy, A. Jha, D. Sen, D. Banerjee, K. K. Chattopadhyay, *J. Mater. Chem. C* **2014**, 2, 7608.
- [64] K. Yu, P. Wang, G. Lu, K.-H. Chen, Z. Bo, J. Chen, *J. Phys. Chem. Lett.* **2011**, 2, 537.
- [65] Y. Qi, B. Deng, X. Guo, S. Chen, J. Gao, T. Li, Z. Dou, H. Ci, J. Sun, Z. Chen, R. Wang, L. Cui, X. Chen, K. Chen, H. Wang, S. Wang, P. Gao, M. H. Rummeli, H. Peng, Y. Zhang, Z. Liu, *Adv. Mater.* **2018**, 30, 1704839.
- [66] G. Sato, T. Morio, T. Kato, R. Hatakeyama, *Jpn. J. Appl. Phys.* **2006**, 45, 5210.
- [67] Q. Yan, F. E. Alam, J. Gao, W. Dai, X. Tan, L. Lv, J. Wang, H. Zhang, D. Chen, K. Nishimura, L. Wang, J. Yu, J. Lu, R. Sun, R. Xiang, S. Maruyama, H. Zhang, S. Wu, N. Jiang, C.-T. Lin, *Adv. Funct. Mater.* **2021**, 31, 2104062.
- [68] Z. Wu, Y. Zhang, Y. Shen, W. Zhang, G. Shao, *Adv. Mater. Interfaces* **2020**, 7, 2000854.
- [69] L. Lin, L. Sun, J. Zhang, J. Sun, A. L. Koh, H. Peng, Z. Liu, *Adv. Mater.* **2016**, 28, 4671.
- [70] M. Li, D. Liu, D. Wei, X. Song, D. Wei, A. T. S. Wee, *Adv. Sci.* **2016**, 3, 1600003.
- [71] I. J. Ford, *Phys. Rev. E* **1997**, 56, 5615.
- [72] Y. Ma, H. Jang, S. J. Kim, C. Pang, H. Chae, *Nanoscale Res. Lett.* **2015**, 10, 308.
- [73] J. Zhao, M. Shaygan, J. Eckert, M. Meyyappan, M. H. Rummeli, *Nano Lett.* **2014**, 14, 3064.
- [74] Y. Ma, W. Jiang, J. Han, Z. Tong, M. Wang, J. Suhr, X. Chen, L. Xiao, S. Jia, H. Chae, *ACS Appl. Mater. Interfaces* **2019**, 11, 10237.
- [75] M. Zhu, J. Wang, B. C. Holloway, R. A. Outlaw, X. Zhao, K. Hou, V. Shutthanandan, D. M. Manos, *Carbon* **2007**, 45, 2229.
- [76] K. Davami, M. Shaygan, N. Kheirabi, J. Zhao, D. A. Kovalenko, M. H. Rummeli, J. Opitz, G. Cuniberti, J.-S. Lee, M. Meyyappan, *Carbon* **2014**, 72, 372.
- [77] V. A. Krivchenko, V. V. Dvorkin, N. N. Dzbanovsky, M. A. Timofeyev, A. S. Stepanov, A. T. Rakhimov, N. V. Suetin, O. Y. Vilkov, L. V. Yashina, *Carbon* **2012**, 50, 1477.
- [78] A. Malesevic, R. Vitchev, K. Schouteden, A. Volodin, L. Zhang, G. V. Tendeloo, A. Vanhulsel, C. V. Haesendonck, *Nanotechnology* **2008**, 19, 305604.
- [79] H. Ci, H. Ren, Y. Qi, X. Chen, Z. Chen, J. Zhang, Y. Zhang, Z. Liu, *Nano Res.* **2018**, 11, 3106.
- [80] Z. Wu, Y. Zhang, L. Li, Y. Zhao, Y. Shen, S. Wang, G. Shao, *J. Mater. Chem. A* **2020**, 8, 23248.
- [81] S. B. Roy, L. Truong, J. H. Jeon, S. Lee, S.-K. Jerng, E. Jung, S. Chan Jun, S.-H. Chun, *ACS Appl. Energy Mater.* **2021**, 4, 5697.
- [82] H. Yang, J. Yang, Z. Bo, S. Zhang, J. Yan, K. Cen, *J. Power Sources* **2016**, 324, 309.
- [83] H. Xu, Y. Yu, Z. Wang, G. Shao, *Energy Environ. Mater.* **2019**, 2, 234.
- [84] L. Tao, Y. Wang, Y. Zou, N. Zhang, Y. Zhang, Y. Wu, Y. Wang, R. Chen, S. Wang, *Adv. Energy Mater.* **2019**, 10, 1901227.
- [85] F. Banhart, J. Kotakoski, A. V. Krasheninnikov, *ACS Nano* **2011**, 5, 26.
- [86] S. Sahoo, G. Sahoo, S. M. Jeong, C. S. Rout, *J. Energy Storage* **2022**, 53, 105212.
- [87] C. Xu, S. Wu, G. Xiong, X. Guo, H. Yang, J. Yan, K. Cen, Z. Bo, K. (K.) Ostrikov, *Appl. Catal. B Environ.* **2021**, 280, 119461.
- [88] A. J. Pak, E. Paek, G. S. Hwang, *Carbon* **2014**, 68, 734.
- [89] Q. Yang, Z. Xiao, D. Kong, T. Zhang, X. Duan, S. Zhou, Y. Niu, Y. Shen, H. Sun, S. Wang, L. Zhi, *Nano Energy* **2019**, 66, 104096.
- [90] I.-Y. Jeon, S. Zhang, L. Zhang, H.-J. Choi, J.-M. Seo, Z. Xia, L. Dai, J.-B. Baek, *Adv. Mater.* **2013**, 25, 6138.
- [91] C. Tsounis, X. Lu, N. M. Bedford, B. Subhash, L. Thomsen, Q. Zhang, Z. Ma, K. (K.) Ostrikov, A. Bendavid, J. A. Scott, R. Amal, Z. Han, *ACS Nano* **2020**, 14, 11327.
- [92] Z. Liu, Z. Zhao, Y. Wang, S. Dou, D. Yan, D. Liu, Z. Xia, S. Wang, *Adv. Mater.* **2017**, 29, 1606207.
- [93] S. Ghosh, K. Ganesan, S. R. Polaki, T. R. Ravindran, N. G. Krishna, M. Kamruddin, A. K. Tyagi, *J. Raman Spectrosc.* **2014**, 45, 642.
- [94] K. Gong, F. Du, Z. Xia, M. Durstock, L. Dai, *Science* **2009**, 323, 760.
- [95] X. Sun, Y. Zhang, P. Song, J. Pan, L. Zhuang, W. Xu, W. Xing, *ACS Catal.* **2013**, 3, 1726.
- [96] D. Li, B. Ren, Q. Jin, H. Cui, C. Wang, *J. Mater. Chem. A* **2018**, 6, 2176.
- [97] J. Zhang, L. Dai, *Angew. Chem., Int. Ed.* **2016**, 55, 13296.
- [98] C. H. Choi, S. H. Park, S. I. Woo, *ACS Nano* **2012**, 6, 7084.
- [99] Y. Su, Z. Yao, F. Zhang, H. Wang, Z. Mics, E. Cánovas, M. Bonn, X. Zhuang, X. Feng, *Adv. Funct. Mater.* **2016**, 26, 5893.
- [100] M. Li, L. Zhang, Q. Xu, J. Niu, Z. Xia, *J. Catal.* **2014**, 314, 66.
- [101] Q. Cao, H. Gao, Y. Gao, J. Yang, C. Li, J. Pu, J. Du, J. Yang, D. Cai, Z. Pan, C. Guan, W. Huang, *Adv. Funct. Mater.* **2021**, 31, 2103922.
- [102] J. P. McClure, J. D. Thornton, R. Jiang, D. Chu, J. J. Cuomo, P. S. Fedkiw, *J. Electrochem. Soc.* **2012**, 159, F733.
- [103] P. Zhai, X. Xuan, H. Li, C. Li, P. Li, M. Li, *Carbon* **2022**, 189, 71.
- [104] X. Xia, S. Deng, D. Xie, Y. Wang, S. Feng, J. Wu, J. Tu, *J. Mater. Chem. A* **2018**, 6, 15546.
- [105] Z. Gao, W. Yang, J. Wang, N. Song, X. Li, *Nano Energy* **2015**, 13, 306.
- [106] S. Imai, H. Kondo, H. Cho, H. Kano, K. Ishikawa, M. Sekine, M. Hiramatsu, M. Ito, M. Hori, *J. Phys. Appl. Phys.* **2017**, 50, 40LT01.
- [107] F. Yu, K. Wang, L. Cui, S. Wang, M. Hou, F. Xiong, R. Zou, P. Gao, H. Peng, Z. Liu, *Adv. Mater.* **2022**, 34, 2110565.
- [108] D. Su, D. Han Seo, Y. Ju, Z. Han, K. Ostrikov, S. Dou, H.-J. Ahn, Z. Peng, G. Wang, *NPG Asia Mater* **2016**, 8, 286.
- [109] S. Ghosh, K. Ganesan, S. R. Polaki, T. Mathews, S. Dhara, M. Kamruddin, A. K. Tyagi, *Appl. Surf. Sci.* **2015**, 349, 576.
- [110] J. Li, Z. Liu, Q. Guo, S. Yang, A. Xu, Z. Wang, G. Wang, Y. Wang, D. Chen, G. Ding, *J. Mater. Chem. C* **2019**, 7, 5995.
- [111] Y. Zhang, Z. Wu, S. Wang, N. Li, S. R. P. Silva, G. Shao, P. Zhang, *InfoMat* **2022**, 4, 12294.
- [112] V. Krivchenko, P. Shevnnin, A. Pilevsky, A. Egorov, N. Suetin, V. Sen, S. Evlashin, A. Rakhimov, *J. Mater. Chem.* **2012**, 22, 16458.
- [113] Z. Bo, W. Ma, P. Wang, E. Wu, W. Yang, K. Yu, X. Zhang, J. Yan, K. Cen, *Phys. Status Solidi B* **2014**, 251, 155.
- [114] C. Y. Cheng, K. Teii, *IEEE Trans. Plasma Sci.* **2012**, 40, 1783.
- [115] S. Mori, T. Ueno, M. Suzuki, *Diam. Relat. Mater.* **2011**, 20, 1129.
- [116] Z. Wang, M. Shoji, H. Ogata, *Appl. Surf. Sci.* **2011**, 257, 9082.

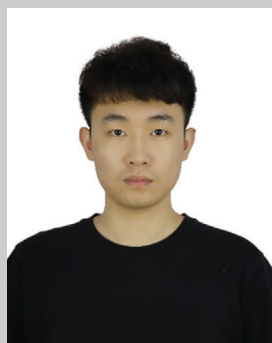
- [117] C. Yang, H. Bi, D. Wan, F. Huang, X. Xie, M. Jiang, *J. Mater. Chem. A* **2012**, *1*, 770.
- [118] Y. Wang, R. Shi, L. Shang, L. Peng, D. Chu, Z. Han, G. I. N. Waterhouse, R. Zhang, T. Zhang, *Nano Energy* **2022**, *96*, 107046.
- [119] C. Hu, Y. Lin, J. W. Connell, H.-M. Cheng, Y. Gogotsi, M.-M. Titirici, L. Dai, *Adv. Mater.* **2019**, *31*, 1806128.
- [120] X. Feng, X. Shi, J. Ning, D. Wang, J. Zhang, Y. Hao, Z.-S. Wu, *eScience* **2021**, *1*, 124.
- [121] H.-F. Yen, Y.-Y. Horng, M.-S. Hu, W.-H. Yang, J.-R. Wen, A. Ganguly, Y. Tai, K.-H. Chen, L.-C. Chen, *Carbon* **2015**, *82*, 124.
- [122] G. Ren, X. Pan, S. Bayne, Z. Fan, *Carbon* **2014**, *71*, 94.
- [123] H. Qi, S. Yick, O. Francis, A. Murdock, T. Van Der Laan, K. (K.). Ostrikov, Z. Bo, Z. Han, A. Bendavid, *Energy Storage Mater.* **2020**, *26*, 138.
- [124] Y. Zhou, X. Cheng, F. Huang, Z. Sha, Z. Han, J. Chen, W. Yang, Y. Yu, J. Zhang, S. Peng, S. Wu, A. Rider, L. Dai, C. H. Wang, *Carbon* **2021**, *172*, 272.
- [125] Y. Cao, X. Meng, A. Li, *Energy Environ. Mater.* **2021**, *4*, 363.
- [126] B. Tang, L. Gao, J. Liu, S.-H. Bo, Z. Xie, J. Wei, Z. Zhou, *J. Mater. Chem. A* **2020**, *8*, 18087.
- [127] S. Li, Z. Wang, J. Liu, L. Yang, Y. Guo, L. Cheng, M. Lei, W. Wang, *ACS Appl. Mater. Interfaces* **2016**, *8*, 19438.
- [128] R. Mo, F. Li, X. Tan, P. Xu, R. Tao, G. Shen, X. Lu, F. Liu, L. Shen, B. Xu, Q. Xiao, X. Wang, C. Wang, J. Li, G. Wang, Y. Lu, *Nat. Commun.* **2019**, *10*, 1474.
- [129] S. Zhang, S. Li, Y. Lu, *eScience* **2021**, *1*, 163.
- [130] Q. Xiao, M. Gu, H. Yang, B. Li, C. Zhang, Y. Liu, F. Liu, F. Dai, L. Yang, Z. Liu, X. Xiao, G. Liu, P. Zhao, S. Zhang, C. Wang, Y. Lu, M. Cai, *Nat. Commun.* **2015**, *6*, 8844.
- [131] J. He, N. Wang, Z. Cui, H. Du, L. Fu, C. Huang, Z. Yang, X. Shen, Y. Yi, Z. Tu, Y. Li, *Nat. Commun.* **2017**, *8*, 1172.
- [132] C. Wang, Y.-S. Chui, R. Ma, T. Wong, J.-G. Ren, Q.-H. Wu, X. Chen, W. Zhang, *J. Mater. Chem. A* **2013**, *1*, 10092.
- [133] X. Liu, D. Wang, B. Zhang, C. Luan, T. Qin, W. Zhang, D. Wang, X. Shi, T. Deng, W. Zheng, *Electrochim. Acta* **2018**, *268*, 234.
- [134] J. Tang, X. Peng, T. Lin, X. Huang, B. Luo, L. Wang, *eScience* **2021**, *1*, 203.
- [135] Z. Wu, X. Zhang, L. Deng, Y. Zhang, Z. Wang, Y. Shen, G. Shao, *Energy Environ. Mater.* **2021**, *5*, 285.
- [136] D. Xie, X. Xia, Y. Zhong, Y. Wang, D. Wang, X. Wang, J. Tu, *Adv. Energy Mater.* **2017**, *7*, 1601804.
- [137] Z. Xia, H. Sun, X. He, Z. Sun, C. Lu, J. Li, Y. Peng, S. Dou, J. Sun, Z. Liu, *Nano Energy* **2019**, *60*, 385.
- [138] J. Liu, Y. Zhang, L. Zhang, F. Xie, A. Vasileff, S.-Z. Qiao, *Adv. Mater.* **2019**, *31*, 1901261.
- [139] C. Li, Z. Sun, T. Yang, L. Yu, N. Wei, Z. Tian, J. Cai, J. Lv, Y. Shao, M. H. Rummeli, J. Sun, Z. Liu, *Adv. Mater.* **2020**, *32*, 2003425.
- [140] C. Lu, Z. Gao, B. Liu, Z. Shi, Y. Yi, W. Zhao, W. Guo, Z. Liu, J. Sun, *Adv. Funct. Mater.* **2021**, *31*, 2101233.
- [141] Y. Mu, Y. Chen, B. Wu, Q. Zhang, M. Lin, L. Zeng, *Adv. Sci.* **2022**, *9*, 2203321.
- [142] Y. Zhang, P. Zhang, B. Li, S. Zhang, K. Liu, R. Hou, X. Zhang, S. R. P. Silva, G. Shao, *Energy Storage Mater.* **2020**, *27*, 159.
- [143] H. Ci, J. Cai, H. Ma, Z. Shi, G. Cui, M. Wang, J. Jin, N. Wei, C. Lu, W. Zhao, J. Sun, Z. Liu, *ACS Nano* **2020**, *14*, 11929.
- [144] Y.-C. Wang, W. Huang, L.-Y. Wan, J. Yang, R.-J. Xie, Y.-P. Zheng, Y.-Z. Tan, Y.-S. Wang, K. Zaghbi, L.-R. Zheng, S.-H. Sun, Z.-Y. Zhou, S.-G. Sun, *Sci. Adv.* **2022**, *8*, eadd8873.
- [145] T. Wu, S. Sun, J. Song, S. Xi, Y. Du, B. Chen, W. A. Sasangka, H. Liao, C. L. Gan, G. G. Scherer, L. Zeng, H. Wang, H. Li, A. Grimaud, Z. J. Xu, *Nat. Catal.* **2019**, *2*, 763.
- [146] C.-C. Weng, J.-T. Ren, H.-Y. Wang, X.-W. Lv, Y.-J. Song, Y.-S. Wang, L. Chen, W.-W. Tian, Z.-Y. Yuan, *Appl. Catal. B Environ.* **2022**, *307*, 121190.
- [147] H. Yang, Y. Liu, X. Liu, X. Wang, H. Tian, G. I. N. Waterhouse, P. E. Kruger, S. G. Telfer, S. Ma, *eScience* **2022**, *2*, 227.
- [148] H. B. Tao, J. Zhang, J. Chen, L. Zhang, Y. Xu, J. G. Chen, B. Liu, *J. Am. Chem. Soc.* **2019**, *141*, 13803.
- [149] C. Lei, Q. Zheng, F. Cheng, Y. Hou, B. Yang, Z. Li, Z. Wen, L. Lei, G. Chai, X. Feng, *Adv. Funct. Mater.* **2020**, *30*, 2003000.
- [150] W. Li, L. Zhao, X. Jiang, Z. Chen, Y. Zhang, S. Wang, *Adv. Funct. Mater.* **2022**, *32*, 2207727.
- [151] J. Kosco, M. Bidwell, H. Cha, T. Martin, C. T. Howells, M. Sachs, D. H. Anjum, S. Gonzalez Lopez, L. Zou, A. Wadsworth, W. Zhang, L. Zhang, J. Tellam, R. Sougrat, F. Laquai, D. M. Delongchamp, J. R. Durrant, I. McCulloch, *Nat. Mater.* **2020**, *19*, 559.
- [152] C. Xu, Z. Bo, S. Wu, Z. Wen, J. Chen, T. Luo, E. Lee, G. Xiong, R. Amal, A. T. S. Wee, J. Yan, K. Cen, T. S. Fisher, K. (K.) Ostrikov, *Sol. Energy* **2020**, *208*, 379.
- [153] B. Dunn, H. Kamath, J.-M. Tarascon, *Science* **2011**, *334*, 928.
- [154] Z. González, S. Vizireanu, G. Dinescu, C. Blanco, R. Santamaría, *Nano Energy* **2012**, *1*, 833.
- [155] W. Li, Z. Zhang, Y. Tang, H. Bian, T.-W. Ng, W. Zhang, C.-S. Lee, *Adv. Sci.* **2016**, *3*, 1500276.



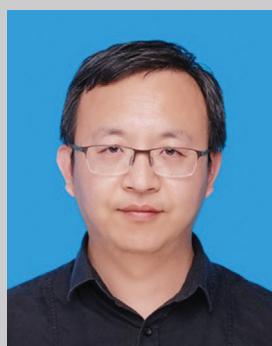
Zhiheng Wu acquired his Ph.D. degree in 2022 under the supervision of Prof. Guosheng Shao in the School of Materials Science and Engineering at Zhengzhou University. He joined the faculty at Zhengzhou University as a lecturer in 2022. His current research focuses on synthesis of graphene-based films for energy storage and conversion applications.



Erhao Wang is enrolled as a master's student in the School of Materials Science and Engineering at Zhengzhou University in 2021 under the supervision of Prof. Guosheng Shao, and his research topic is graphene-based direct methanol fuel cells.



Gongkai Zhang obtained his master's degree in 2023 under the supervision of Associate Professor Yonglong Shen in the School of Materials Science and Engineering at Zhengzhou University. His research focuses on heteroatom-doped vertical graphene and its electrocatalytic application.



Yonglong Shen received his B.S. degree and M. S. degree in Materials Science from Zhengzhou University in 2006 and 2009, respectively. He came to the UK in 2010 and received a PhD degree in Materials Science from the University of Bolton (with Prof. Guosheng Shao) in 2015. He then spent two years as a postdoctoral fellow in Prof. Guosheng Shao's lab at Zhengzhou University and has been an associate Prof. since 2022. His research interests include semiconductors, thin films, electrical and optical properties of metal oxides, solar cells, and advanced characterization techniques (TEM and EELS).



Guosheng Shao is Professor and the Director of the State Centre for International Cooperation on Designer Low-carbon and Environmental Materials (CDLCEM). He is also Founding Director of the Zhengzhou Materials Genome Institute (ZMGI, 2016), and Visiting Professor to the University of Surrey, UK (2018). He earned his PhD in materials science at the University of Surrey in 1995 and thereupon worked as a research fellow and senior research fellow, until transferring to the Brunel University as Reader in Materials in 2005. He joined the University of Bolton as Professor of Materials Modeling and Simulation in 2007, and then established the Institute for Renewable Energy and Environmental Technologies (IREET, 2011) as its founding Director, together with the responsibility as Head of Engineering etc. His academic interest is "designer" materials and application devices, using a materials genome approach to facilitate cost-effective development of novel materials. His current focus is mainly on sustainable (renewable) energy systems and environmental technologies.